National Laser Users' Facility and External Users' Programs

During FY06, 680 target shots were taken on OMEGA for external users' experiments, accounting for 48.8% of the total OMEGA shots for the year. The external users during this year included seven collaborative teams participating in the National Laser Users' Facility (NLUF) program and many collaborative teams from the National Laboratories (LLNL, LANL, and SNL) and the Commissariat à l'Énergie Atomique (CEA) of France. Some of this work is highlighted in this section.

NLUF Program

In FY06, the Department of Energy (DOE) issued a solicitation for NLUF grants for the period of FY07–FY08. A total of 12 proposals were submitted to DOE for the NLUF FY07/08 program. An independent DOE Technical Evaluation Panel comprised of Prof. Ani Aprahamian (University of Notre Dame), Dr. Steven Batha (LANL), Dr. Ramon Leeper (SNL), Prof. Howard Milchberg (University of Maryland), and Dr. Robert Turner (LLNL) reviewed the proposals on 18 April 2006 and recommended that six of the twelve proposals receive DOE funding and shot time on OMEGA in FY07–FY08. Table 108.VIII lists the successful proposals.

FY06 NLUF Experiments

FY06 was the second of a two-year period of performance for the NLUF projects approved for the FY05–FY06 funding and OMEGA shots. Six of these NLUF projects were allotted OMEGA shot time and received a total of 122 shots on OMEGA in FY06. Some of this work is summarized in this section.

Isentropic Compression Experiments (ICE) for Measuring EOS on OMEGA

Principal Investigators: Y. M. Gupta and J. R. Asay (University of Washington)

This experimental effort is geared toward developing new areas of high-pressure research. The aim of the FY06 shots was to continue development of techniques to generate high-accuracy, quasi-isentrope, equation-of-state data. This will make possible, for the first time, "cold" stress-density loading curves for standard materials at loading rates up to ten times higher than possible with other methods in the Mbar regime. For the FY05 NLUF allocation, a platform was developed to produce high-accuracy and high-pressure stress-strain data on aluminum.[1] This was the first such data to be measured with a

Table 108.VIII: FY07–FY08 NLUF Proposals.

Principal Investigator	Affiliation	Proposal Title
R. P. Drake	University of Michigan	Experimental Astrophysics on the OMEGA Laser
R. Falcone	University of California, Berkeley	X-Ray Compton Scattering on Compressed Matter
P. Hartigan	Rice University	Laboratory Experiments on Supersonic Astrophysical Flows Interacting with Clumpy Environments
R. Jeanloz	University of California, Berkeley	Recreating Planetary Core Conditions on OMEGA—Techniques to Produce Dense States of Matter
R. Mancini	University of Nevada, Reno	Multiview Tomographic Study of OMEGA Direct-Drive Implosion Experiments
R. D. Petrasso, C. K. Li	Massachusetts Institute of Technology	Monoenergetic Proton Radiography of Laser/Plasma-Generated Fields and ICF Implosions

laser driver and was taken with ramp compression timescales more than ten times faster than had previously been possible. A stiffer response of aluminum was observed than had been previously observed at slower ramp compression experiments on the Z facility at Sandia National Laboratory. In addition, it was observed that the elastic–plastic transition is much larger than expected from previous work at Z. This points to a strong rate dependence in the material strength. The new high-strain-rate data provided by these experiments are being used to benchmark models that incorporate time dependence being developed at Washington State University (WSU).

On 26 April 2006, 14 shots were performed on isentropic compression targets. The ICE-EOS package, as shown in Fig. 108.58, consists of a Au hohlraum, a plastic reservoir followed by a vacuum gap, and a triple-stepped Ta target. Fifteen beams from the OMEGA laser at 0.35-μm wavelength, containing a combined energy of 5 kJ in a 2-ns temporally flat pulse, are focused symmetrically onto the inner walls of the Au hohlraum (1.7-mm LEH, 2.2-mm diameter, 1.7-mm length). This confined high-Z geometry results in a near-blackbody distribution of thermal x rays (T_h ~ 120 eV) with uniform temperature gradients over a spatial region close to the diameter of the hohlraum. The hohlraum is attached to a 25-μm-thick Be foil glued to a 180-μm-thick, 12% Br-doped polystyrene foil ($C_8H_6Br_2$). The x-ray field within the hohlraum launches an ablatively driven shock through the foil. The initial region of planarity is expected to approach the diameter of the halfraum and can extend over millimeters. The Bromine dopant absorbs high-energy Au M-band x rays (~2 to 5 keV) generated within the hohlraum, which otherwise could preheat the Ta step sample. After breakout from the rear-surface shock, heating and momentum cause the Br-CH to dissociate and unload across a 600-μm vacuum gap. Transit across the vacuum gap causes the mass-density gradients along the target axis to relax as a function of distance from the original Br-CH/vacuum-gap interface. The unloading Br-CH monotonically loads up against the Ta sample, and the imparted momentum launches a ramp stress wave through the material. The temporal profile of the compression wave may be shaped by varying the size of the vacuum gap, the density of the reservoir, or the temperature within the hohlraum. In the FY06 experiments the main targets consisted of 25/40/55/70 μm Ta or W. A significant change in the target design from the previous campaigns in FY05 was the inclusion of a Be ablator and 1-μm CH liner on the inner wall of the Au hohlraum. The purpose of this modification was to keep the hohlraum open for ~80 ns to facilitate future on-axis radiography experiments that would diagnose material properties (e.g., material strength) during compression. In this context an "open" hohlraum means no on-axis, line-of-sight Au content that would serve to absorb the flash x-ray photons used for radiography. Be has a high-ablation velocity, and its inclusion (1) increases the x-ray ablative shock pressure into the sample for a given input laser energy and (2) serves to fill the holhraum rapidly and thus acts as a filler, which delays the on-axis stagnation of the cylindrically converging Au holhraum material. The 1-μm-CH liner serves to further tamp the hohlraum collapse. The primary goal of the FY06 NLUF shots was to use this planar drive to extract a single-shot series of equation-of-state (EOS) data for Ta and W up to peak pressures in excess of 1 Mbar.

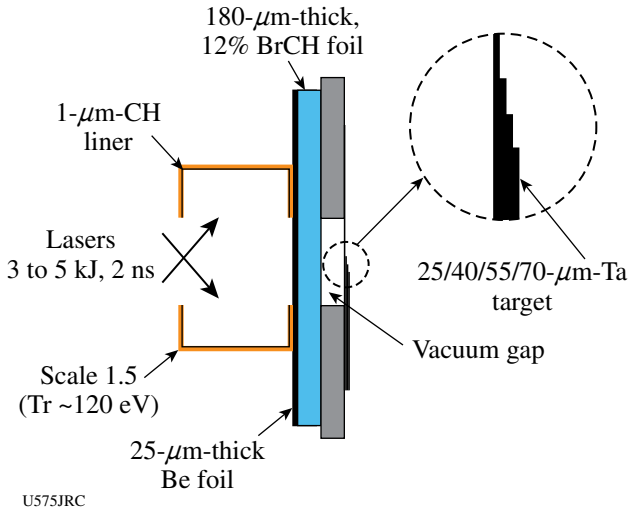

Figure 108.58
Schematic of ICE–EOS target package. The inclusion of a Be ablator and a 1-mm CH liner material serves to keep the hohlraum open for ~100 ns, as was verified in a separate radiography campaign.

The time history of the Ta/vacuum interface acceleration is recorded with a line-imaging velocity interferometer [velocity interferometry system for any reflector (VISAR)] with two channels set at different sensitivities. The time-resolved fringe movement recorded by a streak camera is linearly proportional to the velocity of the reflecting surface, which in this case is the Ta/vacuum interface. This allows an accurate measurement of the free-surface velocity as a function of time. The streak camera output of the VISAR for the target conditions described in Fig. 108.58 is shown in Fig. 108.59. The recently upgraded LLE VISAR provides a greater target field of view than had previously been possible, thereby allowing the use of four separate steps on a single shot for the first time, which ultimately increases the accuracy of the equation-of-state measurement.

The VISAR image provides spatial resolution at the target plane over ~800 μm and temporal resolution of the interferometer fringe displacement over a 30-ns time window. A planar

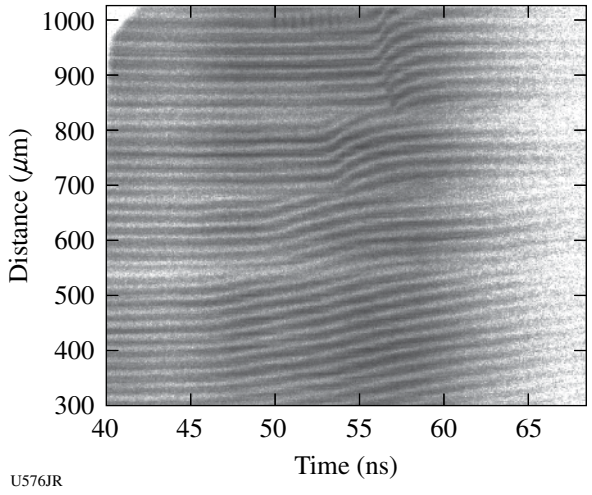

Figure 108.59
VISAR streak record for target conditions described in Fig. 108.58.

drive was observed across the field of view with smooth ramp unloading from the 25-, 40-, 55-, and 70-μm-Ta samples at progressively later times. The velocity sensitivity (set by the resolving element within the VISAR) is 0.995 km s^{-1} fringe shift^{-1}. Using Fourier analysis and after deconvolving the data for temporal and spatial distortions within the streak camera, the time-resolved free-surface velocity (U_{FS}) profile for each Ta thickness (Fig. 108.60) can be extracted. There is a very pronounced elastic–plastic precursor wave on all steps. An increase in this elastic–plastic wave as a function of Ta thickness/ramp rise time is observed. This is an important observation that points to a rate dependence in the material response. Analysis of this data is ongoing.

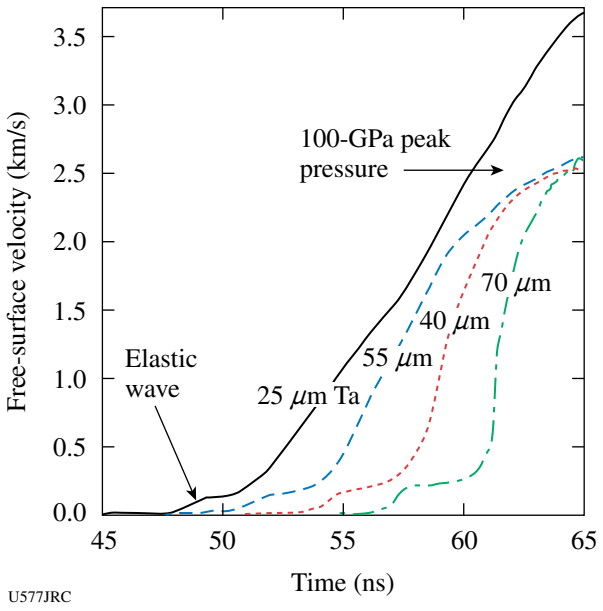

Figure 108.60
Free-surface velocity profile deduced from the data in Fig. 108.59.

Using the iterative analysis technique described by Rothman *et al.*,[2] the free-surface velocity profiles in Fig. 108.60 can be used to generate a path through stress-density space up to 1 Mbar (Ref. 1). In future experiments techniques will be developed to shape the pressure profile of the ramp compression wave by using graded density reservoir materials.[3] This will increase the shock-up distance within the target, which in turn will facilitate larger step heights resulting in lower error bars. In addition, the use of graded density reservoirs is expected to increase the accessible peak pressure on OMEGA to greater than 4 Mbar.

Laser–Plasma Interactions in High-Energy-Density Plasmas
Principal Investigator: H. Baldis (University of California, Davis)

High-temperature hohlraums (HTH) are designed to reach high radiation temperatures by coupling a maximum amount of laser energy into a small target in a short time. These 400- to 800-μm-diam gold cylinders fill rapidly with hot plasma during irradiation with multiple beams in 1-ns laser pulses. The high-Z plasmas are dense, (electron density n_e/n_c ~ 0.1 to 0.4), hot (electron temperature T_e ~ 10 keV), and bathed in a high-temperature radiation field (radiation temperature T_{rad} ~ 300 eV). Here the critical density n_c equals 9×10^{21}/cm^3. The laser beams heating this plasma are intense (~10^{15} to 10^{17} W/cm^2). The coupling of the laser to the plasma is a rich regime for laser–plasma interaction (LPI) physics. The LPI mechanisms in this study include beam deflection and forward scattering. To understand the LPI mechanisms, the plasma parameters must be known. An L-band spectrometer is used to measure the electron temperature. A ride-along experiment is to develop the x-radiation emitted by the thin back wall of the half-hohlraum into a thermal radiation source.

Figure 108.61 shows the experimental setup. About twenty laser beams in three cone angles are incident into a 600-μm-diam, 660-μm-long half-hohlraum. The side walls of the hohlraum are gold, usually 20 μm thick. The back wall is thin, ~1 μm of gold or 1 μm of gold overcoated with 1 μm of parylene. The high- and intermediate-angle beams are focused at the center of the laser entrance hole (LEH), but the low-angle beams are focused ~250 to 400 μm in front of the LEH to avoid hitting the back wall. An LPI probe beam is incident almost normal to the hohlraum axis and aimed to an interaction region,

which is the plasma that is 200 μm in front of the LEH. The transmission and forward scatter of this beam are measured with the temporally and spectrally resolved spectrometers and calorimeters in the full-aperture backscatter (FABS) diagnostic. Because of the laser-beam configuration on the OMEGA laser, one can use FABS to measure the forward-scattered light from opposing beams. If the beam is deflected, it falls onto the NBI plate. A time-averaged image of this deflection is recorded by the NBI camera. The L-band spectrometer views the plasma in the LEH region. The x-radiation emitted by the thin back wall can be used to heat a physics target. To characterize this source, the heating of a witness placed ~400 μm outside the back wall (Fig. 108.61) was measured.

Beam deflection is measured with the NBI plate. Figure 108.62 shows images of the NBI plate as a function of LPI probe-beam intensity for two independent interaction beams. As the intensity increases, the beam deflection increases (the cross marks the center of the beam). The LPI beam is "bent" by the plasma flowing out of the target. Beam deflection occurs when the ponderomotively induced density depressions in the plasma move downstream and carry the light refracted into them. The images from NBI 25 and NBI 30 correspond to interaction beams B46 and B61, traversing the plasma at angles 31° and 9°, respectively, with respect to the normal to the axis of symmetry of the hohlraum. The beam deflections at 5×10^{15}W/cm^2 are approximately 15° and 7.2°, respectively. This is the first observation of beam deflection as a function of laser intensity for different optical paths along the plasma.

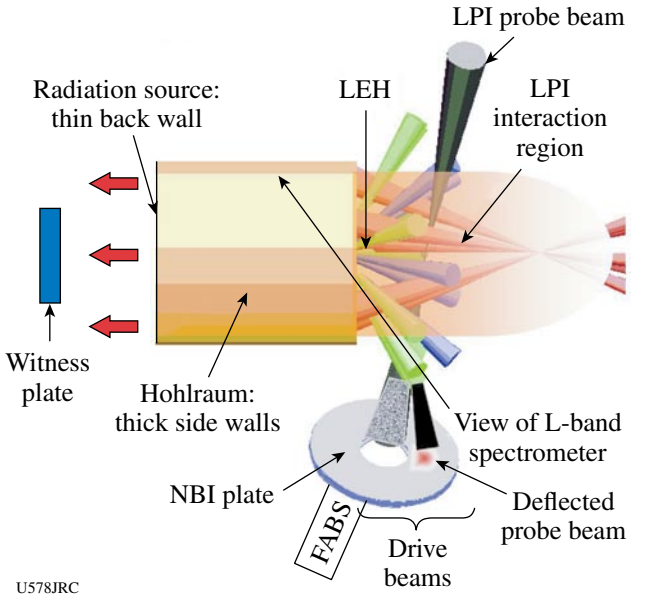

Figure 108.61
Experimental setup of a hot hohlraum experiment.

Understanding the measured LPI mechanisms depends on knowing the plasma parameters. Radiation-hydrodynamics codes are used to predict the plasma conditions. These must be benchmarked by measurements of n_e and T_e. In highly charged gold, the $3d \rightarrow 2p$ transitions of individual ionization states are separated by about 40 eV. If these lines can be resolved, the spectrum gives the distribution of the ionization states of gold. This, combined with models that predict the ionization state as a function of electron temperature, would give T_e.

The L-band spectrometer is designed to measure the $3d \rightarrow 2p$ transitions in gold with high resolution. It is a transmission crystal spectrometer mounted to a single-strip framing camera. It captures a single-time and space-resolved, high-resolution spectrum. Figure 108.63(a) shows a measured spectrum. There is a group of lines, peaking at 10,100 eV, with half-width of about 250 eV. Simulated spectra [Fig. 108.63(b)] from the nonlocal thermodynamic equilibrium (NLTE) code *FLYCHK* (for $\langle Z \rangle$ as a function of electron temperature) and *FLYSPEC* (for spectral lines) show similar features: a group of lines about 200 eV wide. The centroid moves to higher x-ray energy with higher electron temperature. A comparison of the data with simulation shows the measured electron temperature is ~7 to 8 keV.

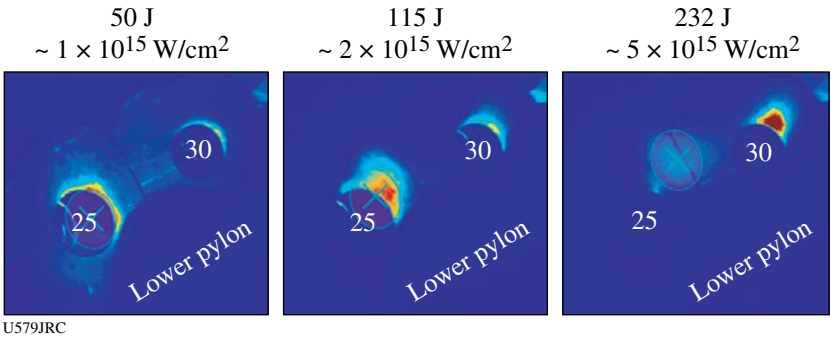

Figure 108.62
Images of NBI plates show beam deflection as a function of LPI probe-beam intensity.

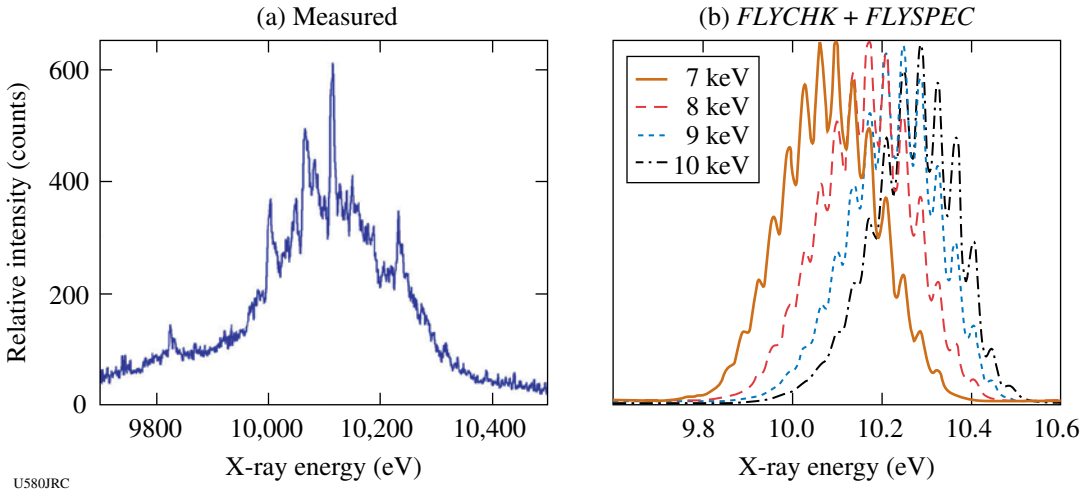

Figure 108.63
(a) L-band spectrometer measurement of $3d \rightarrow 2p$ transitions in Au. (b) Simulated spectra using the code *FLYCHK*.

Measured stimulated Brillouin forward scattering (SBFS) is shown in Fig. 108.64. The SBFS confirms the time at which the plasma reached the interaction region, by the transition from 3ω laser light to SBFS. The absence of 3ω light after 1 ns may indicate that the nonlinear beam deflection has shifted the beam toward the NBI plate, with the light missing the collecting lens. It is possible that the SBFS is *not* deflected because of its lower intensity.

The use of the back wall as a radiation source is demonstrated by using it to heat a Cr witness plate. The arrangement for the HTH half-hohlraum with a witness plate is shown in Fig. 108.65. Figure 108.65(a) shows a schematic of the target. The witness plate (WP) is mounted ~400 μm from the back wall, at an 11° tilt to the back wall so that the imaging diagnostic views the WP edge-on. The WP is a thin chromium foil

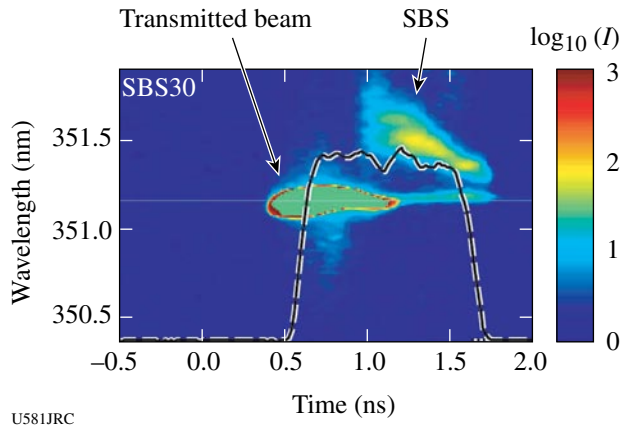

Figure 108.64
Streak camera image showing forward SBS.

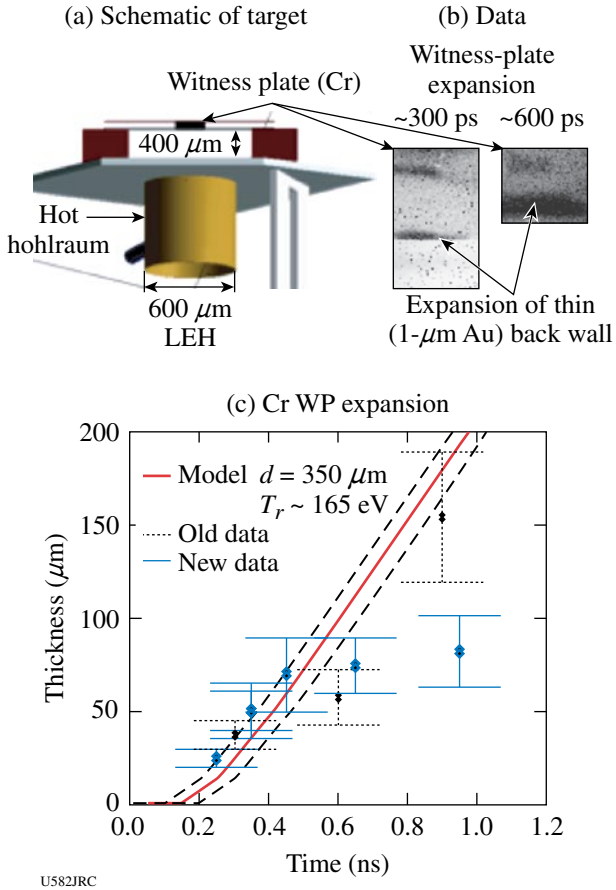

Figure 108.65
New radiation source: the thin back wall of an HTH half-hohlraum is used to heat a witness plate (WP). (a) The sketch of the target shows a WP mounted ~300 μm from the back wall at an 11° angle so it is viewed edge-on by the OMEGA diagnostic. (b) The data show a WP glowing after it has been heated by the back wall (also glowing). (c) The measured expansion of the Cr WP.

sandwiched in plastic (1 μm on each side). Figure 108.65(b) shows the heated WP at two different times. Since these were taken on two different shots, the distance of the WP from the back wall is slightly different; however, the WP is clearly expanding as it is heated. Figure 108.65(c) shows the measured width of the WP as a function of time from several shots on several different days. The solid line is the predicted expansion from a radiation–hydrodynamic simulation, assuming the WP is heated solely by radiation from the back wall. The data are consistent with the simulation, which predicts the radiation temperature in the plate to be ~165 eV.

The following additional measurements of plasma parameters in the LPI region have been performed: (a) the M-shell spectra of gold, (b) Raman backscatter, and (c) 2ω and 4ω Thomson scattering. These data are still being analyzed.

Experimental Astrophysics on the OMEGA Laser
Principal Investigator: R. P. Drake (University of Michigan)
Co-investigators: B. A. Remington, H. F. Robey, S. G. Glendinning, D. D. Ryutov, M. Herrmann, A. R. Miles, A. J. MacKinnon, B. E. Blue, and J. F. Hansen (LLNL); M. Koenig (LULI, Ecole Polytechnique, France); D. Arnett (University of Arizona); R. Rosner and T. Plewa (University of Chicago); J. Stone (Princeton University); S. Bouquet (CEA, France); J. P. Knauer and T. R. Boehly (LLE); Y. Zhang and J. Glimm (SUNY Stony Brook)

The OMEGA laser can address important issues in astrophysics because, through laser ablation, it can produce pressures of tens of Mbars over areas of square millimeters. Two such issues are the contribution of hydrodynamic instabilities to the structure in supernovae and the dynamics of radiative shock waves. After successfully creating collapsed radiative shock structures in both argon and xenon gas, an experiment was performed to Thomson-scatter light from the 4ω beam off of a shock front in argon gas.

In the experiment, ten smoothed beams of the OMEGA laser irradiate a 20-μm beryllium disk with UV light at an irradiance of ~5×10^{14} W/cm^2 for 1 ns. This launches the disk via ablation pressure at a high velocity into a 600-μm-diam, 6-mm-long polyimide tube filled with 1.1 atm (0.001 g/cm^3) of argon gas. This target had openings covered with 3000-Å polyimide facing the 4ω probe beam and the UV spectrometer and streak camera in TIM-2. The scattering volume was 3.7 mm from the initial drive disk position. The 4ω probe beam fired in a 2-ns pulse at 200 J, with a best-focus spot size of 100 μm. The target axis for this experiment was parallel to the probed ion-acoustic waves.

Figure 108.66 shows spectral data from the first experiments to obtain Thomson-scattering data from a shock front. The signal lasted 300 ps, starting at 20.1 ns after the drive beams turned on. Before that, the signal was from the tail end of a destroyer beam blasting off the polyimide cover facing the collection diagnostic in TIM-2. The spectrum of the scattered light and a fit to the data are shown in Fig. 108.67. The overall spectrum is shifted in frequency by a Doppler shift, implying that the flow velocity of the shocked fluid is 110 km/s. Fits to the spectrum using the kinetic theory of Thomson scattering, combined with an evaluation of the average charge using an "average atom" model, give an ion temperature of 300 eV, an electron temperature of 250 eV, and an average charge of 13.7. These are sensible values for the argon near the shock front.

Astrophysical Jets and HED Laboratory Astrophysics
Principal Investigator: P. Hartigan (Rice University)

A variety of objects in the universe are surrounded by accreting disks of matter, and most of these systems drive highly collimated supersonic jets out the poles of these disks. Examples include jets from young stars, planetary nebulae, x-ray binaries, and black holes at the centers of active galaxies. The goal of this

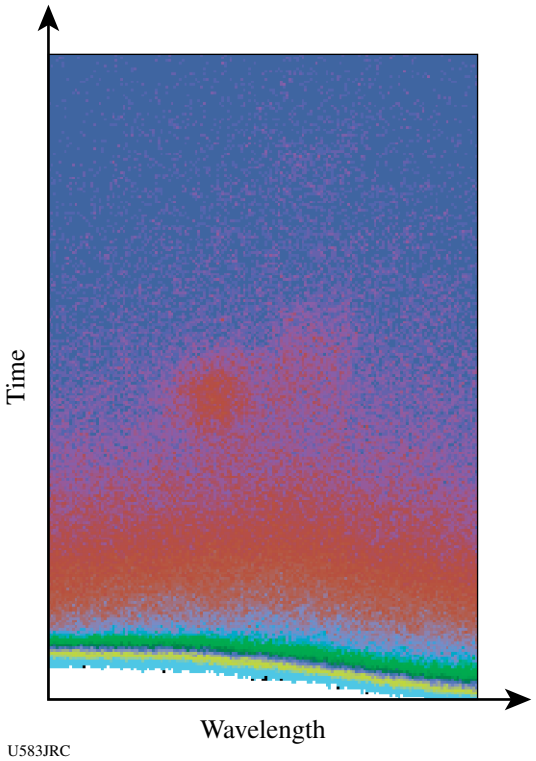

Figure 108.66
Streak camera data showing Thomson-scattered-light spectral evolution for collapsed radiative shock.

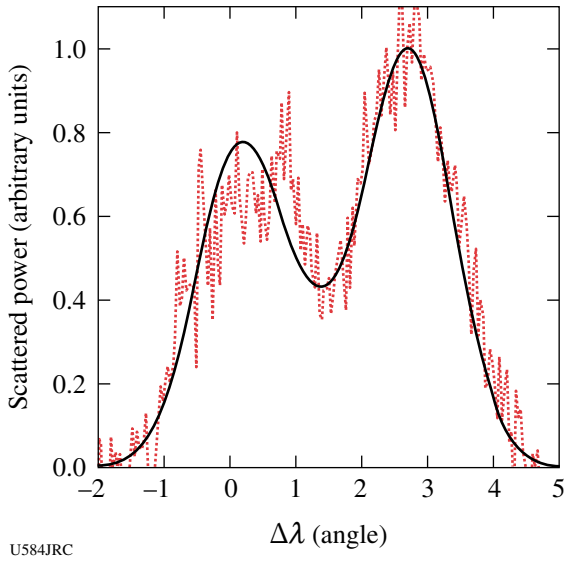

Figure 108.67
Thomson-scattered spectrum and fit to the data for Fig. 108.66.

project is to create laboratory analogs of the jet phenomenon in the laboratory and follow what happens when such a jet interacts with an obstacle in the flow as it is observed to do in many astrophysical situations. An astrophysics fluid dynamics code (*AstroBEAR*) and the *RAGE* code at Los Alamos are both used to help design the experiment and interpret the results.

In the past year, two shot days were allotted for the project, and both succeeded in producing excellent images of shocks in the jet and the ball as the latter was being destroyed and entrained by the flow. The targets consisted of a dense ball embedded at various offset distances (impact parameters) from the axis of the jet. The data set now includes a continuous range of impact parameters and times so we can follow the process as a function of these two variables. Sample images from the experiment are shown in the Fig. 108.68. Astrophysical observations of a deflected jet are scheduled for the end of November, and we will be comparing the new spectra from that effort with numerical datacubes of the *RAGE* and *AstroBEAR* simulations of the laser experiments to improve our understanding of the dynamics of these flows.

Recreating Planetary Core Conditions on OMEGA
Principal Investigator: R. Jeanloz (University of California, Berkeley)

Significant technical as well as scientific breakthroughs in the NLUF high-pressure experiments on planetary fluids were made this past year. The approach that is used involves driving a laser-induced shock wave through a sample already precompressed in a diamond-anvil cell (Fig. 108.69). This combines the benefits of static and dynamic methods of high-pressure experiments, allowing the final pressure–volume–temperature (*P*–*V*–*T*) state of the sample to be tuned across a broad range of thermodynamic conditions (Fig. 108.70). In fact, much-higher compressions, thus more-extreme interatomic interactions, are achieved through this approach than through traditional shock-wave (Hugoniot) measurements.

One of the major technical accomplishments of this program has been the significant improvement of the understanding of

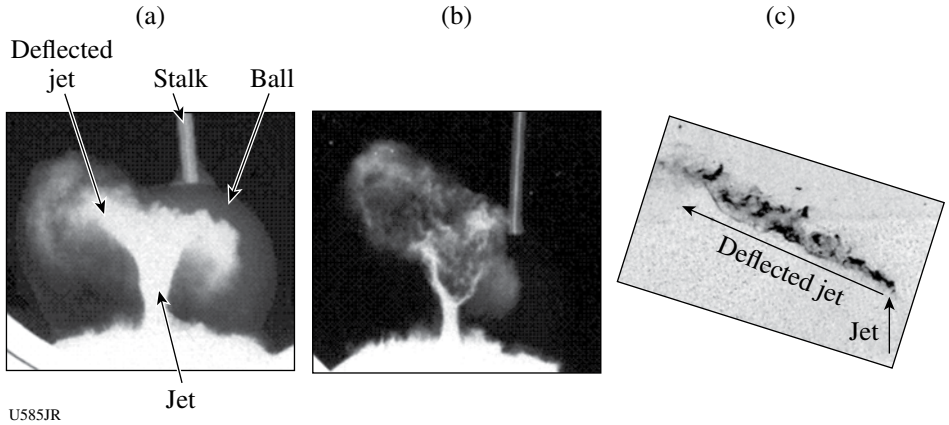

Figure 108.68
Deflected jets in the laboratory and in the universe. (a) OMEGA image of a jet deflecting from a ball located 300 μm from the axis of the jet, at 150 ns, taken with an Fe backlighter. Shocks are clearly visible in the ball and ahead of the deflected jet, which is starting to fragment. (b) Same as (a) with a 350-μm offset at 200 ns and a Zn backlighter. (c) Hubble Space Telescope image of the deflected jet HH 110. The jet emerges from a young star off the bottom of the image and deflects off an opaque dark cloud of gas and dust.

the interferometry records obtained from the shock experiments (Fig. 108.71). Despite the use of antireflection coatings, the components in these experiments generate residual reflections that cause "ghost fringes" to appear in the VISAR records. This source of noise is now understood, to the point that the "ghost fringes" serve as internal calibrants for the records and a joint inversion of the records can be performed to obtain far better velocity resolution than previously thought possible.

In addition to equation-of-state measurements, one of the key measurements obtained from the VISAR records is the optical reflectivity of the shock front: it is possible to determine whether one is looking through the shock front or off its surface by the way the velocity fringes. The reflectivity at optical wavelengths can be converted to an equivalent of electrical conductivity, allowing us to determine the competing P–T conditions under which helium becomes metallic (Fig. 108.72). This is important because the metallization conditions for helium, far more extreme than those for hydrogen, determine the depths at which hydrogen and helium—the primary constituents of giant planets—can behave as metallic alloys. Without such alloying, it is expected that helium separates from the much lighter hydrogen, and the gravitational energy released by this "differentiation" process is thought to be a major source of heat and internal evolution of giant-planetary interiors. Indeed, experiments now underway will allow the documentation of the enhanced reflectivity of hydrogen + helium mixtures (Fig. 108.73), promising to offer significant new constraints on models of planetary evolution and origins.

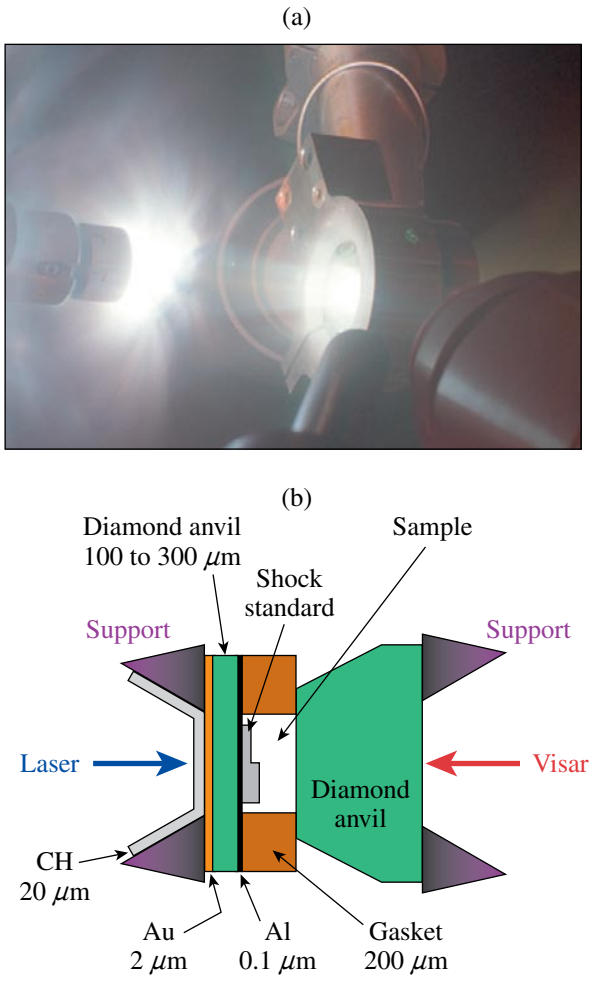

Figure 108.69
Photograph of (a) a loaded diamond cell subjected to laser-shock compression and (b) schematic cross section of the diamond cell. The diamond anvil of the entry (drive-laser) side must be thin in order to minimize attenuation of the shock front before it enters the sample. Diagnostics include velocity interferometry (using VISAR) as well as pyrometry (not shown).

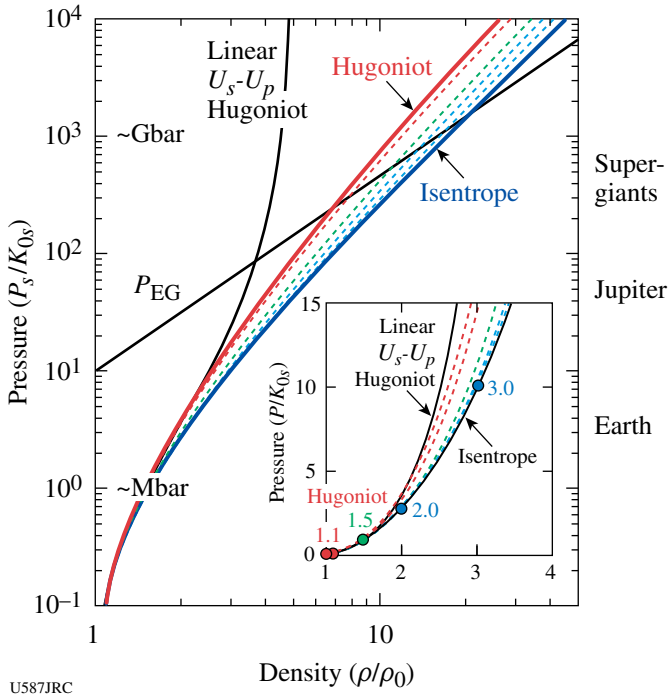

Figure 108.70
Pressure–density (P–ρ) equations of state, normalized by the zero-pressure bulk modulus (K) and density illustrating the range of conditions that can be achieved between the single-shock Hugoniot and isentrope as a function of precompression by factors of 1.1, 1.5, 2.0, and 3.0 (see inset), all calculated from the Birch–Murnaghan[4] and Mie–Grüneisen[5] approaches assuming K'_0 = 4, a Grüneisen parameter varying as γ/ρ = constant, and γ_0 = 1.5 (subscripts 0 and s indicate zero-pressure and isentropic conditions, respectively). The linear shock-velocity U_s versus particle-velocity U_p relationship, and the density dependence of the ideal electron–gas pressure (P_{EG}) are shown for comparison, as are Mbar and Gbar pressures and planetary-center conditions (Earth, Jupiter, and supergiants) corresponding to a typical bulk-modulus value of 100 GPa (= 1 Mbar). The inset shows the lower-pressure range on a linear plot.

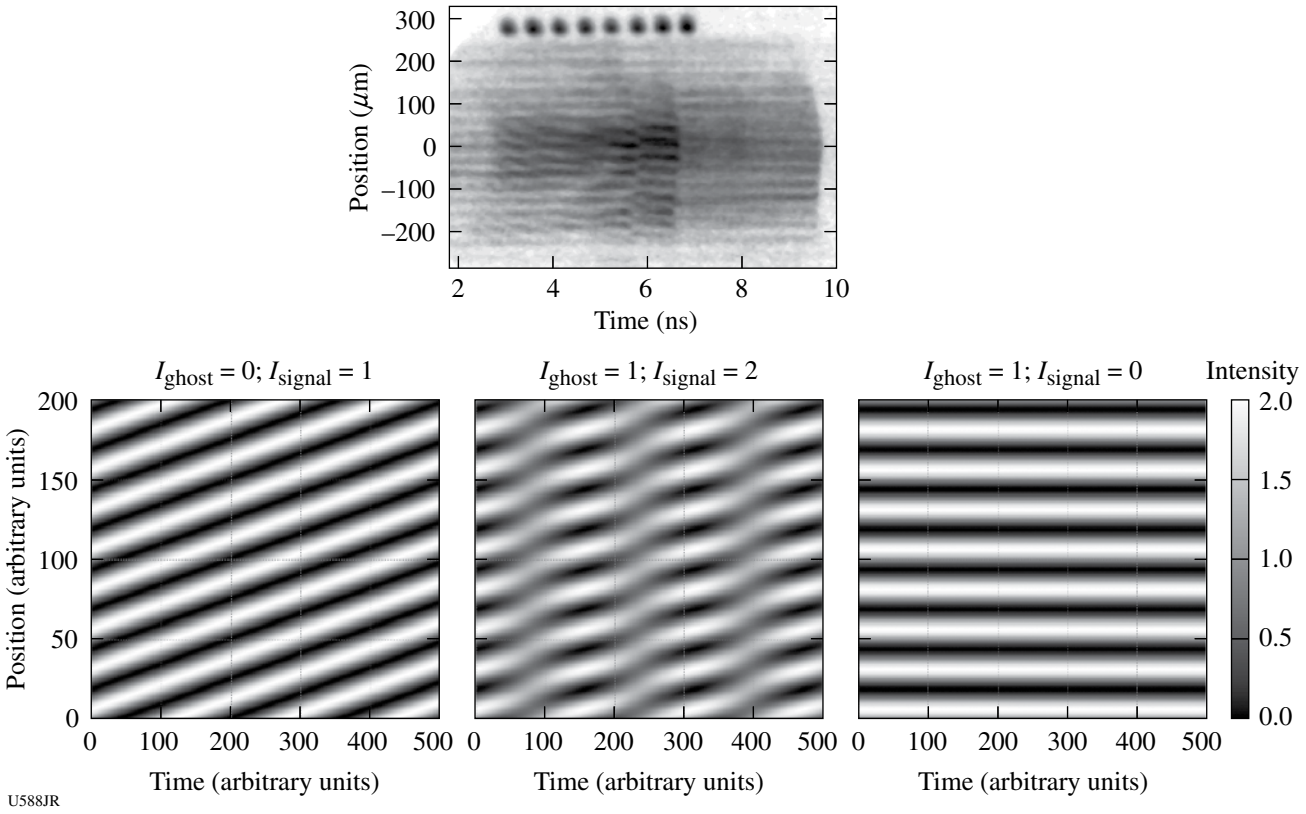

Figure 108.71
(Top) Velocity-interferometry (using VISAR) record from a laser-shock experiment on precompressed helium showing the presence of "ghost fringes" due to residual reflections from diamond and other surfaces. (Bottom) Simulations of the ghost fringes, from 100% signal (no ghost) on the left to 100% ghost (no signal) on the right; center panel shows a 2:1 intensity ratio for signal:ghost.

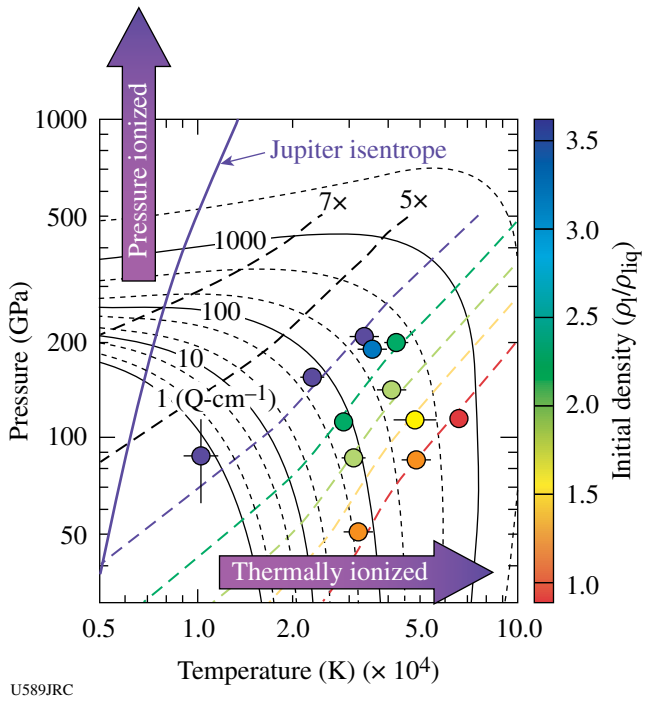

Figure 108.72
Reflectivity measurements as a function of pressure–temperature conditions achieved in helium (circles shaded according to the precompressed density ρ_1 prior to shock loading) quantified in terms of equivalent electrical conductivity (solid and dotted contours). The data clearly probe the trade-offs between pressure and temperature in causing metallization (ionization), with predicted trajectories for different amounts of precompression indicated by the dashed lines and the model temperature distribution (isentrope) inside Jupiter shown for comparison.

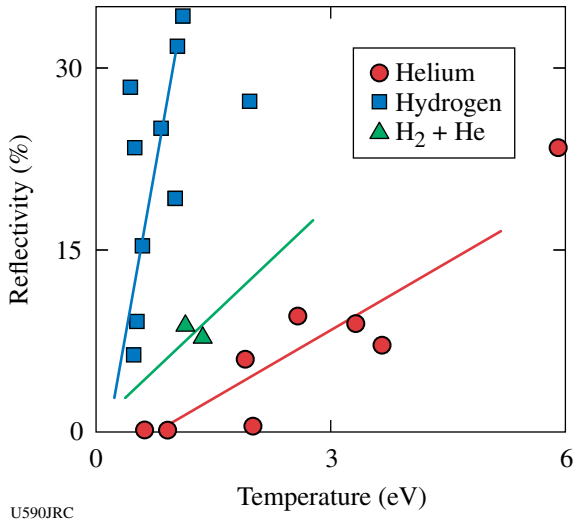

Figure 108.73
High-pressure reflectivity of hydrogen, helium, and hydrogen + helium mixtures under shock compression, shown as a function of Hugoniot temperature determined from pyrometry.

Three-Dimensional Study of the Spatial Structure of Direct-Drive Implosion Cores on OMEGA

Principal Investigator: R. Mancini (University of Nevada, Reno)

The objective of this project is to study the three-dimensional (3-D) structure of the temperature and density spatial profiles of OMEGA direct-drive implosion cores using data from gated narrowband x-ray core images recorded along three quasi-orthogonal directions. To this end, this experiment uses plastic shell targets filled with deuterium gas and a tracer amount of argon for spectroscopic diagnostic purposes. Three identical multimonochromatic imagers (MMI) have been designed, built, and fielded on OMEGA implosion experiments to perform observations along the lines of sight (LOS) of TIM-2, TIM-3, and TIM-4; this set of TIM's represents a quasi-orthogonal system of x-y-z Cartesian axes. The implosions were driven with 60 OMEGA beams, 23 kJ of UV energy, and a 1-ns square laser pulse. At the collapse of the implosion, the hot and dense core plasma achieved temperatures in the 1- to 1.5-keV range and electron number densities in the 1×10^{24} cm^{-3} to 2×10^{24} cm^{-3} range. X-ray K-shell line emission from the argon dopant is a suitable spectroscopy diagnostic for this temperature and density range.

Core images (recorded by MMI instruments) that are formed by a large array of 10-μm-diam pinholes and reflected off a depth-graded WB_4C multilayer mirror with an average bilayer thickness of 15 Å yield narrowband x-ray images in the photon energy range from 3 to 5 keV. They have a magnification of 8.5, provide spatial resolution of approximately 10 μm, and record gated (framed) images characteristic of a 50-ps time interval. Indeed, these instruments record data with simultaneous space, time, and photon energy resolution. As an illustration of the data recorded by MMI, Figs. 108.74 and 108.75 display a time history of narrowband x-ray core images from OMEGA shot 42643 at the collapse of the implosion, based on the argon Ly$_\beta$ ($1s\ ^2S$–$3p\ ^2P$, $h\nu$ = 3936 eV) and He$_\beta$ ($1s^2\ ^1S$–$1s2p\ ^1P$, $h\nu$ = 3684 eV) line emissions. The photon energy narrowband of these images is given by the (mainly) Stark-broadening widths of the line shapes, which for the plasma conditions of these cores is 60 to 70 eV. Core dimensions are in the 60- to 100-μm range. At early times, images recorded along both quasi-orthogonal directions show cores that are large and mostly round. For later times, one LOS shows a core shape that evolves into an oval shape, while the other LOS shows an object that remains more rounded but

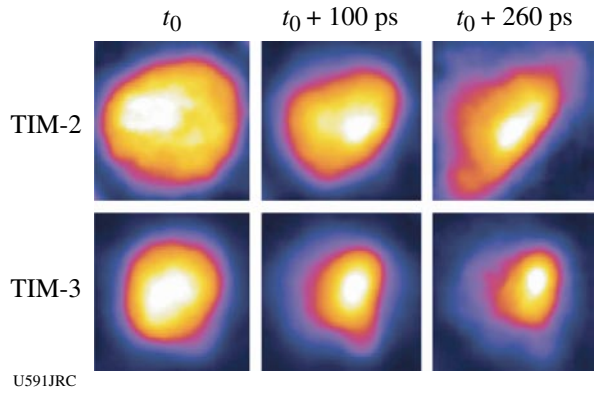

Figure 108.74
Gated argon Ly$_\beta$ narrowband core images recorded along two quasi-orthogonal directions on OMEGA shot 42643.

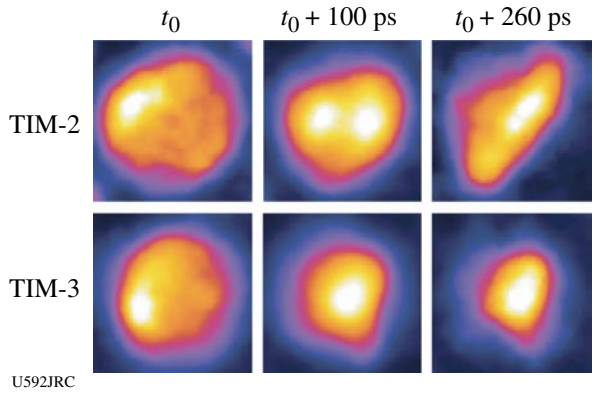

Figure 108.75
Gated argon He$_\beta$ narrowband core images recorded along two quasi-orthogonal directions on OMEGA shot 42643.

getting smaller. Both observations suggest the evolution of a 3-D core from rounded to ellipsoidal shapes with a well-defined orientation in space. It is also interesting to observe the regions of greatest brightness associated with the Ly_β and He_β line emissions, which depends on both temperature and density conditions in the core. Detailed spectral modeling and analysis of the emissivity and opacity of the argon x-ray emission permit a reconstruction of spatial structure of the plasma. In this connection, Fig. 108.76 displays a temperature map based on the analysis of the second frame of data (i.e., t_0 + 100 ps) displayed in Figs. 108.74 and 180.75. The range of values of this spatial profile is consistent with the range of temperatures extracted from the analysis of data independently recorded with streaked spectrometers in the same experiment. Several analysis methods are currently being investigated that simultaneously consider data observed along several LOS's.

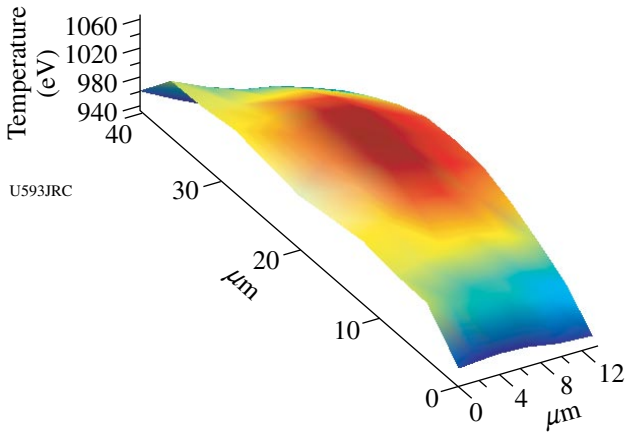

Figure 108.76
Core temperature map for OMEGA shot 42643 extracted from TIM-2 data in Figs. 108.74 and 108.75 for t_0 + 100 ps.

Implosion Dynamics and Symmetry from Proton Imaging, Spectrometry, and Temporal Measurements

Principal Investigators: R. D. Petrasso and C. K. Li (Massachusetts Institute of Technology)

As part of the MIT NLUF program, data was taken in an ongoing series of experiments using proton radiography to study transient *E* and *B* fields generated by the interaction of OMEGA laser beams with plastic foils. High-resolution, time-gated radiography images of a plastic foil driven by a 10^{14}-W/cm^2 laser implied *B* fields of ~0.5 MG and *E* fields of ~1.5 × 10^8 V/m. Simulations of these experiments with *LASNEX* + *LSP* have been performed and are in overall (though not exact) agreement with the data both for field strengths and for spatial distributions; this is the first direct experimental test of the laser-generated *B*-field package in *LASNEX*. The experiments also demonstrated that laser phase plates substantially reduce medium-scale chaotic field structure. The results have recently been published in *Physical Review Letters*[6] and in *Review of Scientific Instruments*.[7]

In each experiment, two plastic foils were illuminated by a single OMEGA laser beam, and a projection radiograph was made of each foil using a backlighter providing monoenergetic 14.7-MeV protons and a CR-39 area detector for image recording. One foil was perpendicular to the backlighter–detector direction, giving a face-on view of the resultant field structure, while the other foil was parallel to the backlighter–detector direction, giving a side-on view. The backlighter was formed by imploding a D^3He-filled, glass-shell capsule with 20 OMEGA laser beams (see Fig. 108.77). Since the burn duration of the D^3He implosion was short (~150 ps) relative to the 1-ns duration of the foil illumination, and the relative timing of the implosion and the foil illumination was adjustable, it was possible to record images at different times relative to the foil illumination.

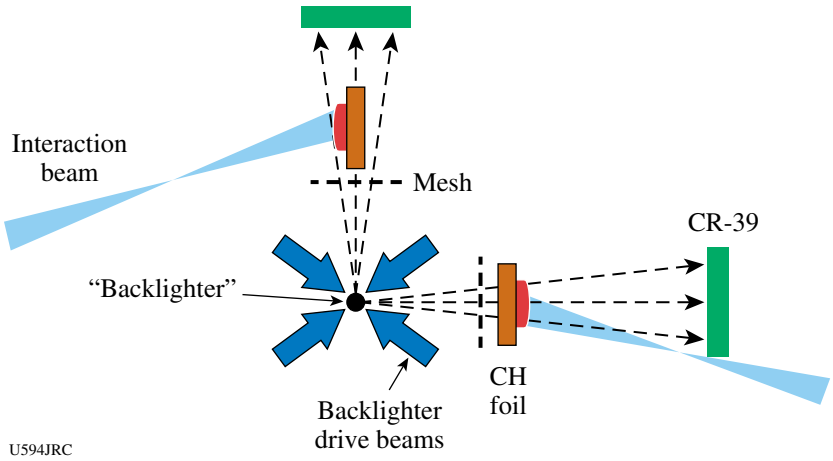

Figure 108.77
Schematic illustration of experimental setup and the physical relationship between the proton backlighter (imploded D^3He-filled capsule), mesh, CH foils, CR-39 imaging detectors, and OMEGA laser beams. The distances of components from backlighter were 0.8 cm for mesh, 1 cm for foil, and 36 cm for detector. The hole-to-hole spacing in the mesh was 150 μm.

The distortion in the mesh pattern at the detector shows how the proton trajectories were deflected through interaction with the fields generated by laser–plasma interaction at the foil. Sample images recorded at different times are shown in Fig. 108.78 (face-on) and Fig. 108.79 (side-on). These images have been analyzed in collaboration with LLNL and LLE to provide information about the time evolution of the field-induced distortion.[6,7]

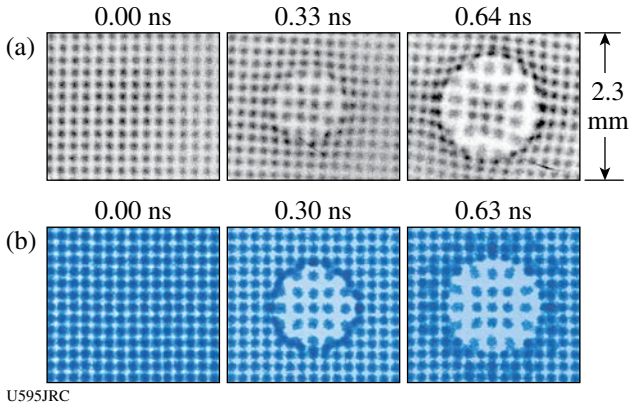

Figure 108.78
(a) Measured face-on D^3He proton images showing the effects of the *B* field generated by laser–plasma interactions at 0.0, 0.33, and 0.64 ns, respectively, after the interaction beam was turned on. The labeled dimensions of the image are scaled to the location of the foil. (b) Images simulated by *LASNEX* + *LSP* for the conditions that produced the experimental images shown in (a).

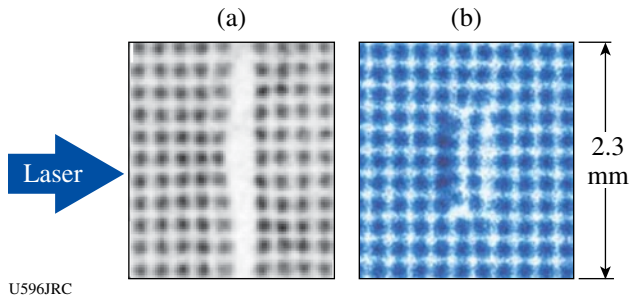

Figure 108.79
(a) Data and (b) simulation for the side-on images. The distortion in the center column of (a) resulted from the *E* field. The large separation between the two center columns of beamlets in (a) is due to attenuation by the CH foil, which is 50 μm thick but 3 mm long in the direction parallel to the proton trajectories; this effect is not seen in (b) because proton–foil interactions were not modeled in the *LSP* simulation.

FY06 LLNL OMEGA Experimental Programs

In FY06 LLNL led 354 shots on the OMEGA system. This total represents a shot rate of approximately 4% higher than nominal (340 shots scheduled for the year), an excellent achievement when one considers that LLNL's programmatic needs frequently dictated difficult reconfigurations from one day to the next, especially during split days.

National Ignition Campaign (NIC) Experiments: One of the first experiments of the year was designed to examine the direct effects of laser-heated gas on an implosion capsule within a gas-filled hohlraum. Plastic hohlraums (to minimize radiation drive) and foam witness balls were used in a NIF-foot-scale experiment. The x-ray backlighting data are shown in Fig. 108.80. Arrows point to regions where there is a departure from spherical symmetry due to pressure from the laser-heated gas that filled the hohlraum.

Several shot days were devoted to the study of collective x-ray scattering from plasmons in warm (10 to 15 eV), dense (2 to 3 $\times$ 10^{23} electrons/cm^3) matter. By fitting the data to theoretical models, the electron density is obtained from the scattered x-ray data and found to be in agreement with simulations.

Throughout FY06 a number of laser–plasma interaction experiments were carried out, some in collaboration with CEA, using a gas-filled hohlraum arranged so that one OMEGA beam (beam 30) could be used as an on-axis probe. Spatially imaged Thomson scattering and a time-resolved transmitted beam diagnostic (3ω TBD) were successfully fielded on OMEGA. Various experimental results are shown in Fig. 108.81 (electron and ion temperatures in the gas as a function of time), Fig. 108.82 (Brillouin scattering reduced as electron temperature increases), and Fig. 108.83 (Raman scattering measured as a function of density for fixed intensity). Experiments using a defocused beam with phase plates showed interaction instabilities decreasing with the average intensity, as predicted. Finally, a semiautomated mechanism for calibration of the near-backscatter plate was fielded and tested.[8]

An albedo (ratio of radiant energy emitted divided by radiant energy absorbed) experiment compared gold hohlraums and "cocktail" (mixtures of gold and uranium) 180-eV hohlraums and found, as predicted, a slight increase for the cocktail case.

In another collaboration with CEA, the OMEGA laser was used in the direct-drive configuration to illuminate spheres of gold, uranium, and a cocktail mixture to measure the conversion of laser energy into x-ray energy. Particular attention was given to obtaining detailed measurements in the 2- to 5-keV range.

An extensive series of experiments were performed for platform development, and use of that platform, for measuring the

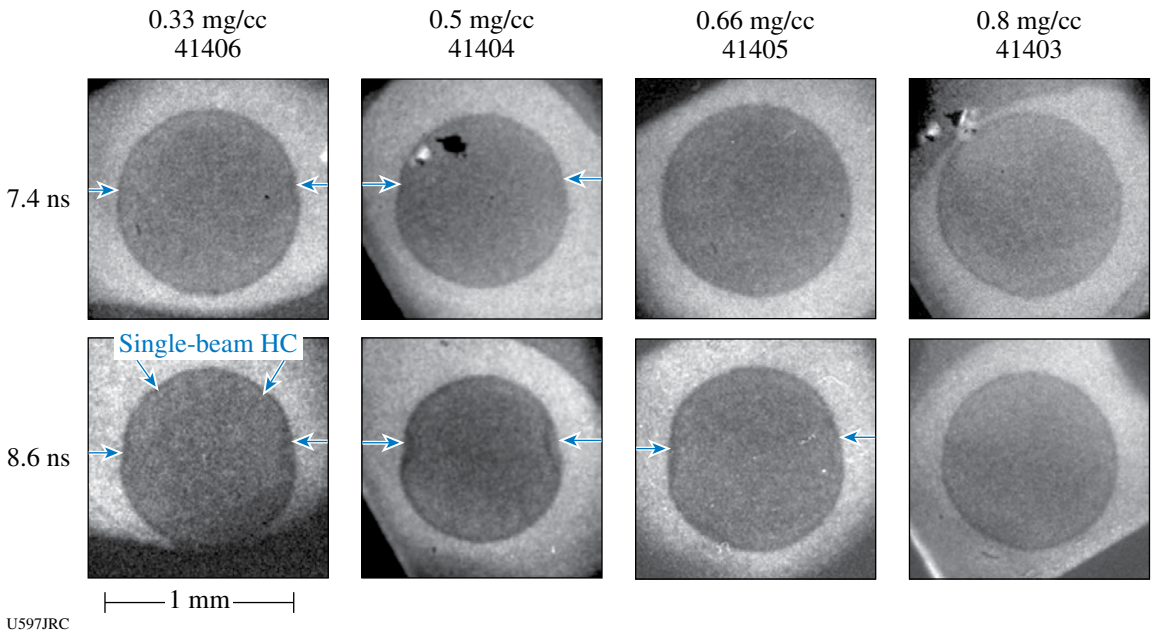

Figure 108.80
X-ray-backlit images of foam spheres, showing (arrows) effects of pressure from laser-heated hohlraum fill gas. Good backlighting foam-ball data were measured for the 0.3- to 0.8-mg/cc hohlraum fill range of interest for HC.

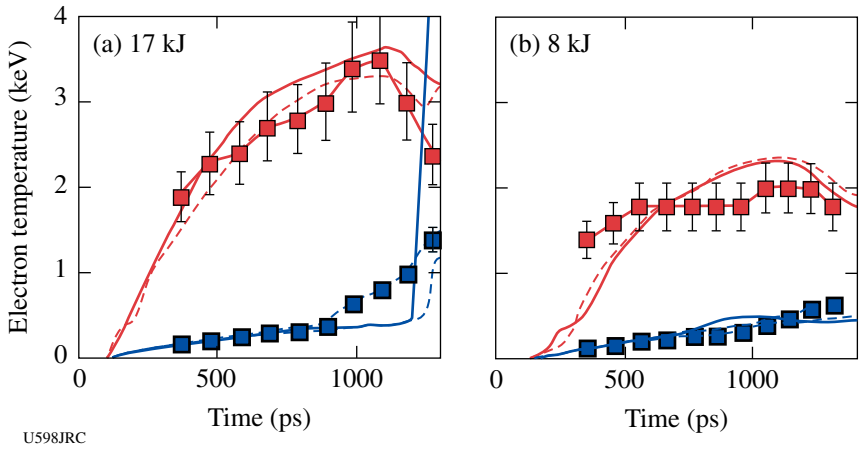

Figure 108.81
Electron temperature (open squares), ion temperature (dark squares), and simulations (solid lines) as a function of time along the laser beam path. The measured electron- and ion-temperature evolution validates the simulations of the plasma conditions along the interaction beam path.

Rayleigh–Taylor growth of ablator materials, being ablatively accelerated by x-ray drive. The planar ablator samples were mounted on the end of a one-ended hohlraum ("halfraum"). X-ray backlighting of the planar samples was used in both side-on and face-on geometry. The latter required imaging through the halfraum. Side-on images were obtained with both 2-D framing cameras and 1-D streak cameras, depending on the experiment. One goal is to be able to measure RT growth in Be from its inherent grain structure; this requires that the platform be capable of nearly 1000× growth, to increase the structure to observable size and simulate expected NIF conditions. Figure 108.84 shows face-on data for two materials, Be and diamond. The initially imposed 1-D perturbations have grown to measurable size. Figure 108.85 shows a summary of these results for diamond. Analysis and simulations are still ongoing to form a more complete understanding of the processes.

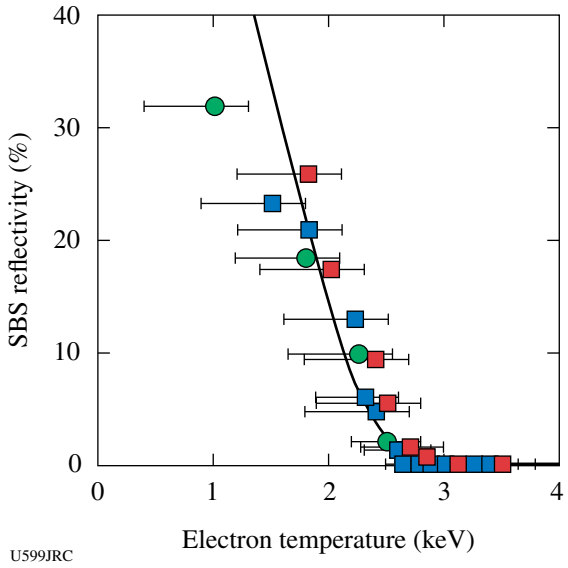

Figure 108.82
Measured SBS reflectivity (points) follows linear gain calculation (solid line) and drops with electron temperature, as predicted. Stimulated Brillouin scattering is reduced to zero for electron temperatures above 2.5 keV.

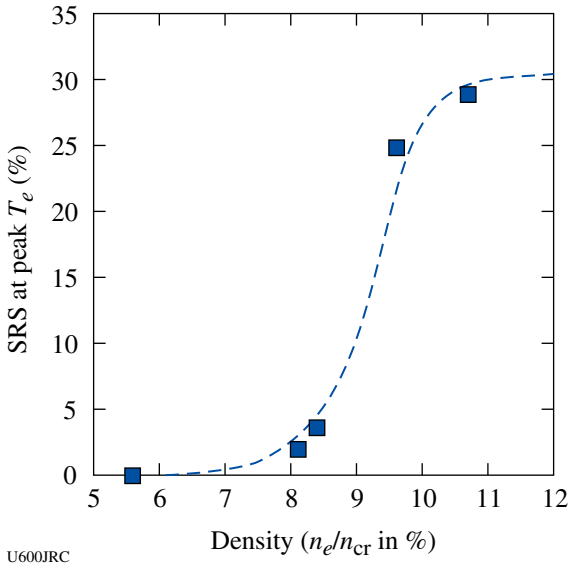

Figure 108.83
Density scaling of SRS at an intensity of 1.5×10^{15} W/cm^{-2}. Raman-scattering levels are consistent with linear gain calculations, varying with electron density for fixed laser intensity.

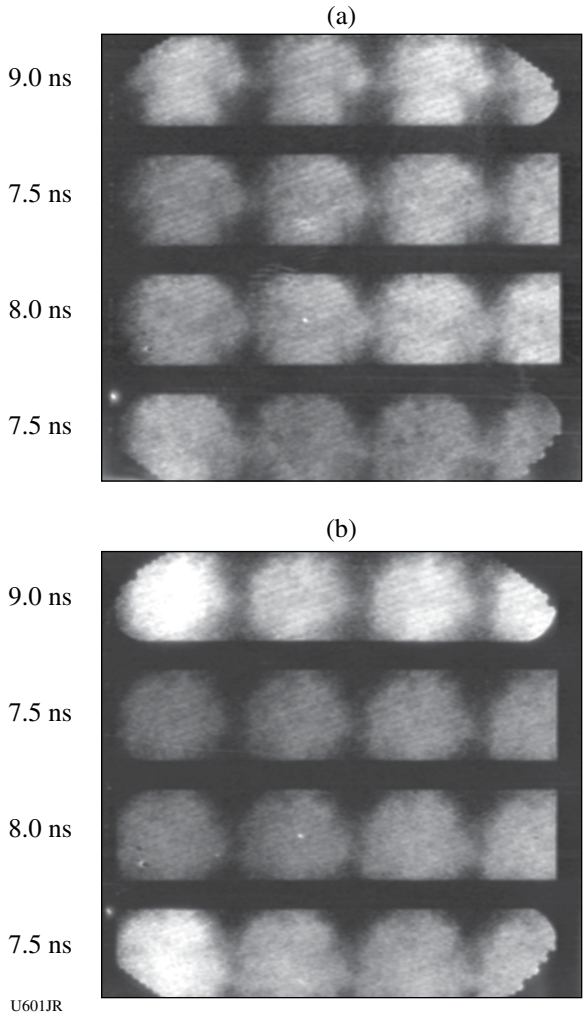

Figure 108.84
X-ray-backlit images of ablatively accelerated planar foils. Observation of large growth of 150-nm amplitude initial perturbations demonstrated (lines running diagonally lower left to upper right) for both (a) carbon (diamond) and (b) Be ablators, as expected, based on previous CH(Ge) results.

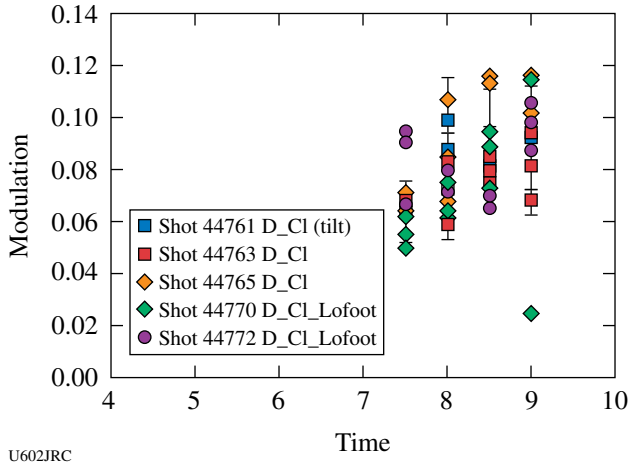

Figure 108.85
Modulation depth for diamond foils (see Fig. 108.84) for various times and laser drives.

A concern with gas-filled hohlraums is that they must, of necessity, have a window to contain the gas. Despite the fact that these windows are thin and low Z, they are the first objects irradiated by the laser beams, and they can generate x rays that may affect the capsule. To obtain quantitative data, Be step wedges (planar Be samples with three different thicknesses) were exposed to x rays produced by the interaction of the OMEGA laser with a thin plastic window. The resulting shock and preheating of the Be were measured with the active shock breakout (ASBO) diagnostic. An example of such data is shown in Fig. 108.86. The termination of the fringes (time runs left to right) coincides with the shock breaking out of the rear surface of the three steps (thickest step at top). Still other experiments used the ASBO, VISAR, and streaked optical pyrometer (SOP) to infer changes in the state—specifically, melting points—of Be and diamond, under varying levels of x-ray preheat and shock compression.

A series of implosion experiments modeled NIF fill tubes with a deliberately placed perturbation on the surface of the capsule. The inner layer of the capsule contained a mid-Z (Ti) dopant. Under certain conditions, the perturbation resulted in a hydrodynamic jet of material moving through the imploded core. This jet was detected by the x-ray emission from the Ti dopant. While this experiment looked at the effect of the tube above the capsule, another experiment ("planar fill tube"), done in collaboration with LANL, investigated the effect of the fill hole using a planar analog. Initial experiments gave promising results using foams as a stand-in for solid DT and showed a jet of the indirectly driven ablator material propagating through the hole.

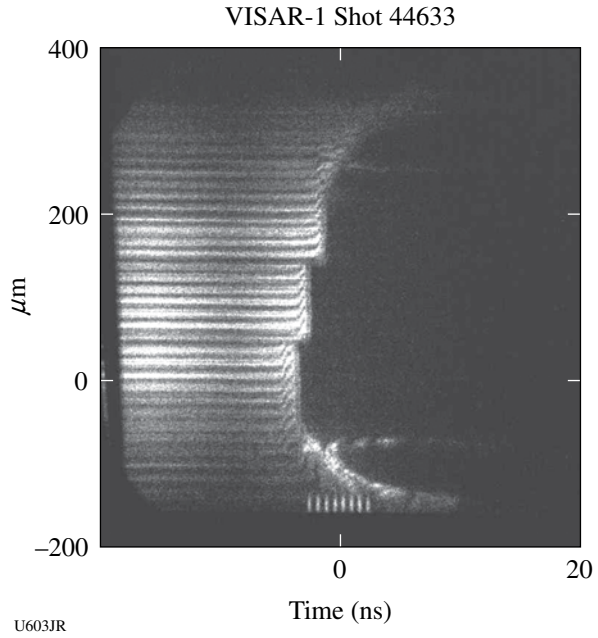

Figure 108.86
ASBO data: shocks in Be driven by x rays from window. The abrupt turnoff of the reflected light (fringes) coincides with the time of shock breakout from the three different thicknesses of Be (thinnest at bottom).

One design for x-ray backlighters on the NIF looks like a peaked roof. Several OMEGA shots were carried out with this geometry to ascertain the x-ray conversion efficiency, and also the spatial uniformity, of this design. The results showed these targets capable of meeting the NIF specifications.

High-Energy-Density Science (HEDS) Experiments: Approximately one third of the LLNL OMEGA shots were for HEDS experiments.

One experiment used very small hohlraums to generate a thermal source of x rays at high photon energies, while at the same time examining the laser–plasma interaction issues associated with such targets. Figure 108.87 shows the x-ray spectra from the 10-keV region, along with model calculations for various thermal temperatures.

Late in FY06 LLNL executed a day of experiments using "double-shell" targets. This represented the culmination of extensive target fabrication work; x-ray tomographic images of the targets are shown in Fig. 108.88. The experiment used a variety of diagnostics, such as time-resolved x-ray backlighting, shown in Fig. 108.89. These data are now undergoing detailed analysis.

The nonlocal thermodynamic equilibrium (NLTE) experiments have as their goal the study and understanding of the radiative effects of high-Z (atomic number) dopants on implosions. Capsules containing deuterium, plus dopant gas, were directly driven by the OMEGA laser. Both spectroscopic x-ray and nuclear diagnostics were employed. Figure 108.90 shows the dramatic order-of-magnitude change in secondary neutrons (those arising as a result of tritium being generated in primary nuclear fusion reactions) observed when a small amount of xenon is added. This is indicative of higher densities in the imploded fuel as a result of radiative cooling from the xenon.

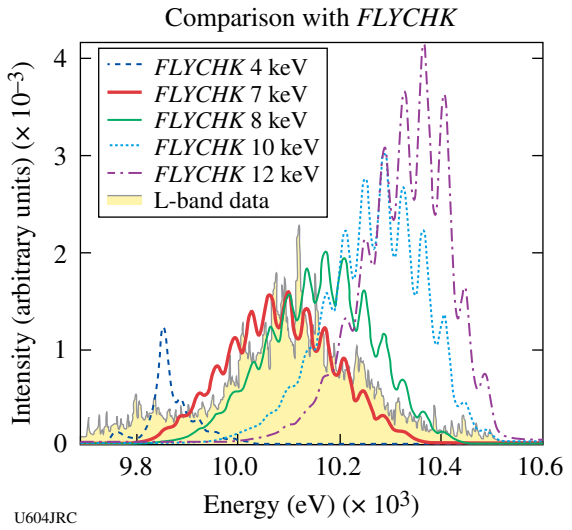

Figure 108.87
Spectroscopic data (gray, shaded area) from small, high-temperature hohlraum are best fit by model calculations (*FLYCHK*) between 7 and 8 keV (between thick and thin solid curves).

Several experiments were carried out to prove the concept of an experimental platform for measuring x-ray opacities in warm, dense matter. These included the development of broadband soft-x-ray backlighters, point backlighters at higher energies, and a hohlraum drive to heat the samples to the desired conditions, along with the necessary diagnostics. These experiments will continue into FY07.

Dynamic hohlraums are directly driven, capsule-within-a-capsule targets. The idea is shown in Fig. 108.91; xenon gas within the outer capsule becomes hot and radiates, causing an x-ray-driven implosion of the inner, deuterium-containing capsule. Data obtained include x-ray-streaked images of the self-emitted x rays, multiple x-ray images, charged-particle information (collaboration with MIT), and multiple standard OMEGA neutron diagnostics. These data are currently being analyzed and compared with simulations.

We continued with our ICE (isentropic compression experiments) in FY06. Various improvements were made to targets, to increase planarity and temporal behavior of the shockless drive. Equation-of-state data were obtained for various materials.

The "shock-sphere" experiment conducted on OMEGA is an example of laboratory astrophysics. In this case, it is model-

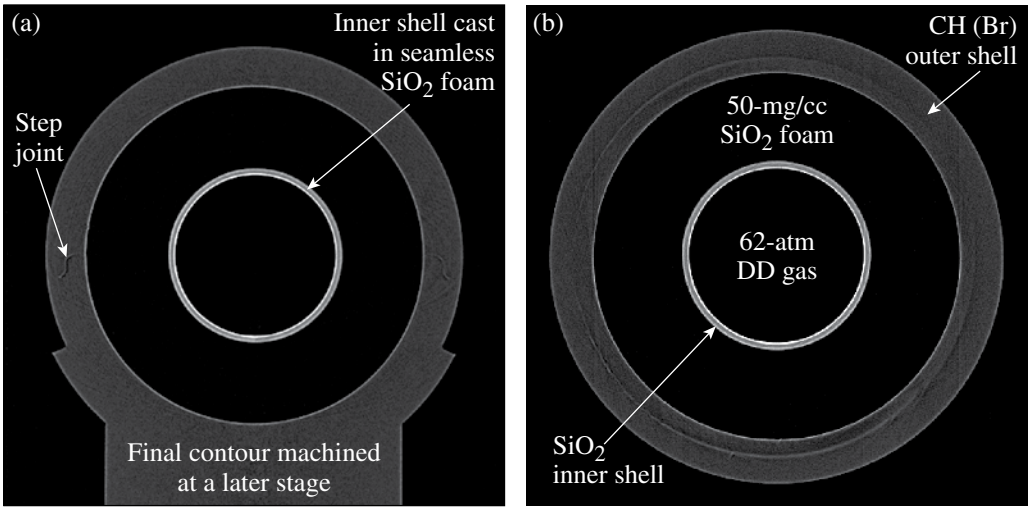

Figure 108.88
SiO_2 double-shell implosions. 3-D tomography of each double-shell capsule was performed to verify that all capsules meet all required specifications.

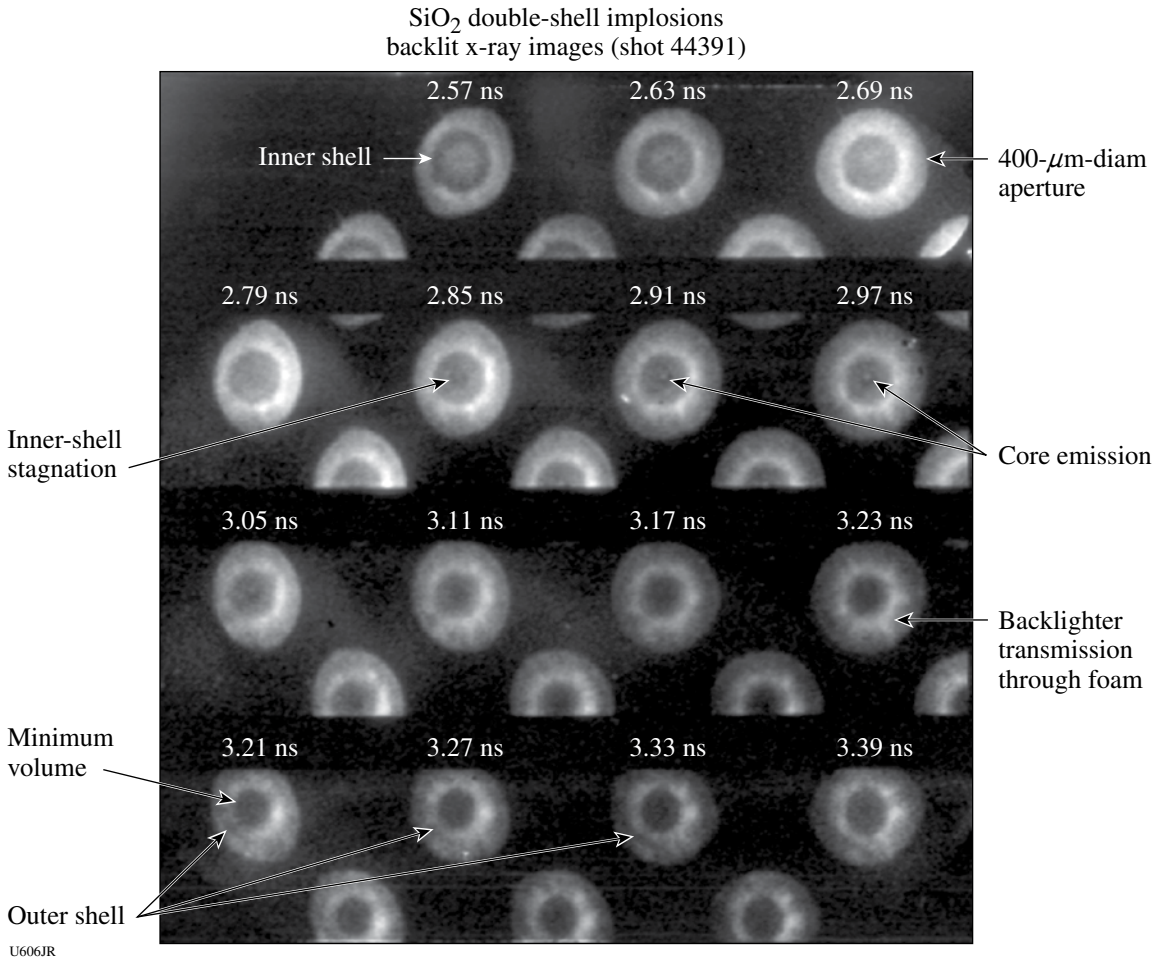

Figure 108.89
Example of backlit x-ray images obtained from double-shell experiments.

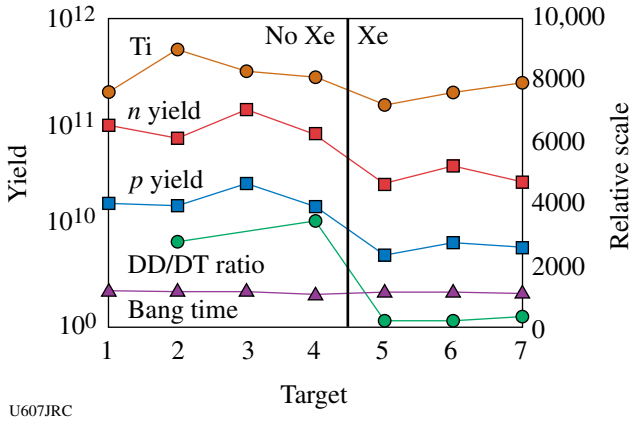

Figure 108.90
Addition of Xe has a significant impact on implosion parameters in NLTE experiments, as shown by neutron data. Note the order-of-magnitude change in DT (secondary) neutrons, due to the radiative cooling by xenon atoms.

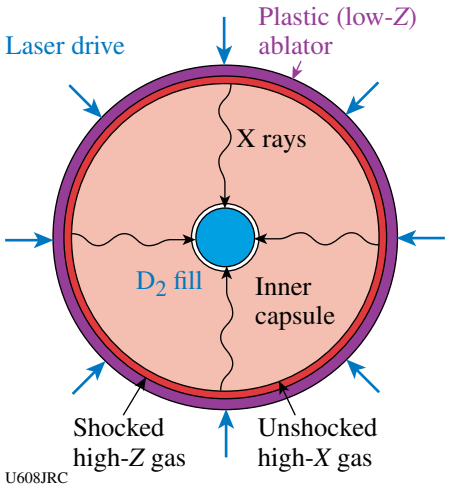

Figure 108.91
Concept of "dynamic hohlraum;" Xe gas between shells produces x rays that ablatively implode inner shell.

ing the passage of a shock in low-density material past denser spherical objects and examining how the shock passage induces mixing of material into the interstellar medium. Figure 108.92 shows an example of the data. The laser-generated shock is moving toward the lower left, past the two spherical objects. (The grid is for diagnostic reference.) X-ray backlighting provides images at various times. On the right (at 12 ns) the shock is still visible, just to the right of the spheres. These data are being used to benchmark model calculations, which will then be applied to astronomical observations for comparison.

Another experiment looked at the propagation of "jets" into a low-density background material ("DDP experiment"), again using x-ray backlighting after lengthy (15- to 35-ns) time delays. The cell size of the low-density material (a copper foam) was varied, and the results compared to simulations. Figure 108.93 shows a schematic of the experiment and an example of the data. As the jet of material moves upward, vortices form to the left and right ("roll up"), in agreement with hydrodynamic simulations.

Finally, another collaboration (CEA, NRL, and LLNL) used OMEGA shots for x-ray source and effects experiments. Various targets were investigated for their ability to produce copious x rays in the region around 10 keV, as shown in Fig. 108.94.

FY06 LANL OMEGA Experimental Programs

Los Alamos National Laboratory (LANL) successfully fielded a range of experiments on OMEGA during FY06 studying the physics relevant to inertial confinement fusion (ICF) and high-energy-density (HED) science in support of the national

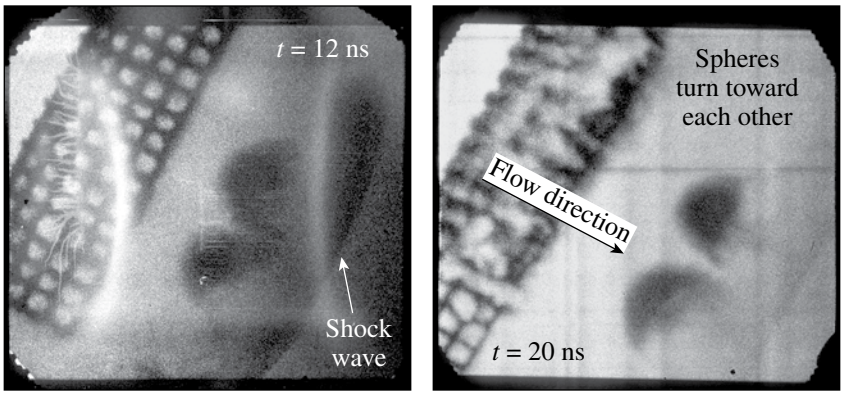

U609JR

Figure 108.92
X-ray-backlit images of shock (visible on right of the right-hand image, moving away from reference grid) and spheres imbedded in the low-density medium. Interacting clouds turn toward each other and eject material downstream after shock passage.

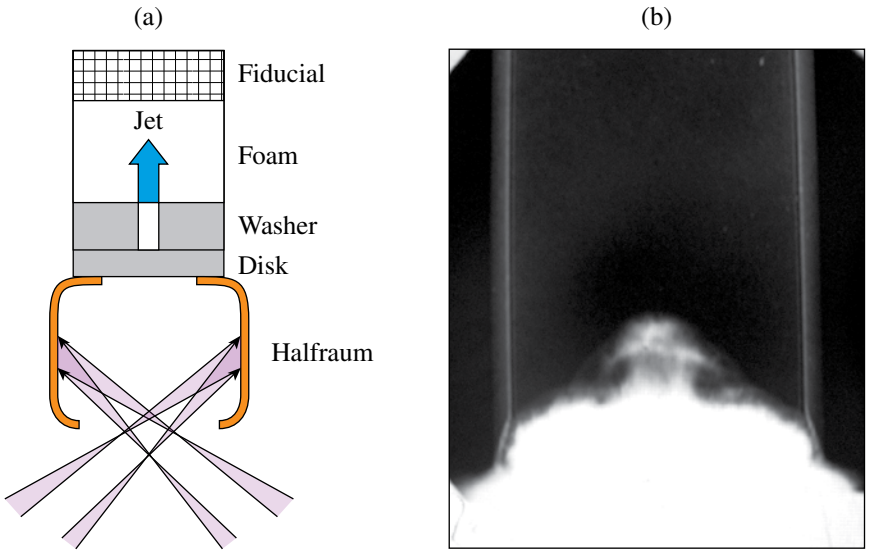

U610JRC

Figure 108.93
(a) Layout of DPP experiment (x-ray backlighting not shown, perpendicular to page through the foam). (b) Data at 15 ns. Note the classic "roll up" of the upward-moving jet.

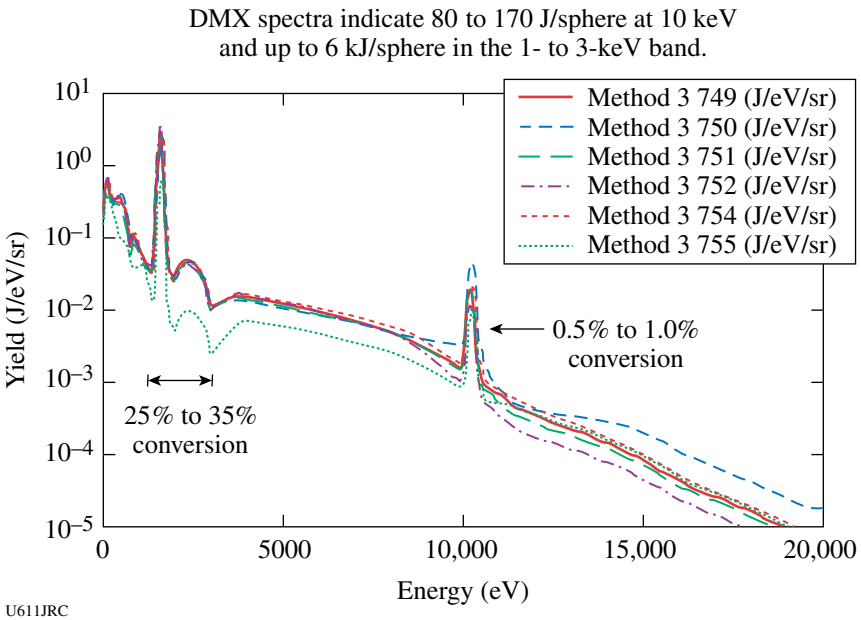

Figure 108.94
Laser and target conditions that optimize the 10-keV x-ray output have been identified.

ignition effort. Many of these experiments were focused on developing underlying physics, diagnostics, and platforms for future experiments on the National Ignition Facility (NIF). LANL conducted a total of 125 target shots on OMEGA. Collaborations with LLNL, LLE, MIT, and AWE remain an important component of LANL's program on OMEGA. With the consolidation of ignition research in the United States into the National Ignition Campaign (NIC), healthy partnerships are required to achieve success in the national scientific objectives.

Off-Hugoniot Heated Hydrodynamics: The off-Hugoniot (OH) campaign continued in FY06 with three days of experiments. High-quality data were obtained on 37 of 39 system shots. These experiments studied material dynamics under heated and shocked conditions. In ignition capsules, defects, arising from the manufacturing process, undergo significant evolution due to heating from Au M-band radiation prior to passage of the main shock. It has not been demonstrated that our hydrocodes accurately capture the physics of this interaction. The OH platform provides the means to study the complex interaction between shocks and heated material.

The OH platform utilizes a beryllium (Be) housing that is coated with a thin layer of tin (Sn). Inside the housing are layers of foam and epoxy. Thirty-three beams strike the tin and produce L-shell radiation that permeates throughout the package, heating the epoxy and foam (Fig. 108.95). A short time later, seven beams launch a strong shock into the foam. As the heated epoxy expands in the foam, the shock interaction with this system is radiographed onto Agfa-D7 film.

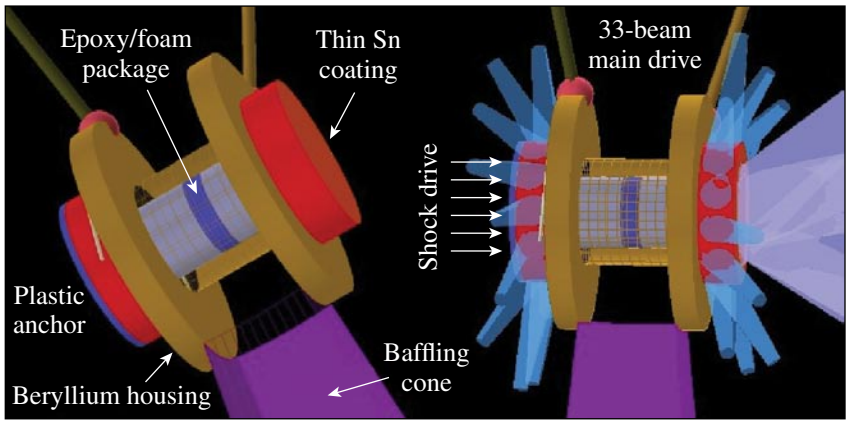

Figure 108.95
The target configuration for the off-Hugoniot experiment. A beryllium housing filled with layers of epoxy and foam is heated by exciting Sn L-shell radiation. The evolution of the epoxy expanding into the foam is imaged via radiography.

An example of the improved data quality is shown in Fig. 108.95. Data from heat-only experiments [Fig. 108.96(a)] clearly show the epoxy expansion and shock in the foam. Moreover, the use of the calibrated D7 film allows complete resolution of the evolving density profiles. When a defect is heated and a strong shock is introduced [Fig. 108.96(b)], the residual density perturbations from the healing defect distort the shock front as it propagates through the epoxy. The resulting density profiles and spatial deformation of the shock front provide tight constraints for our ignition design hydrocodes like *RAGE* and *PETRA*.

Inhomogeneous Radiation Flow: Inhomogeneously mixed materials can occur in a variety of environments. Two examples are ICF capsules, where shell material mixes with the fuel and turbulent flows, and astrophysical systems, such as molecular clouds and star-forming regions, where density clumps can form. Models for the transport of radiation in inhomogenously mixed materials exist, each differing in the statistical treatment of the material mixtures. However, there is little experimental data to test these models. The inhomogeneous radiation flow experiment aims to provide data that can be used to test different models.

Figure 108.97 shows an overview of the experiment. A laser-driven hohlraum is heated to roughly 205 eV, which generates a temperature front. The temperature front propagates through gold-loaded foam, heating it. The soft-emission (~300 eV) of the heated foam is measured to determine the position of the radiation front. Two different gold-doped foams were examined: one loading with gold particles of diameters between 0.3 and 1.0 μm and another with very fine gold particles, diameters less than 0.1 μm.

Figure 108.98 displays preliminary measurements of the temperature-front position (circles) and the simulated trajectory

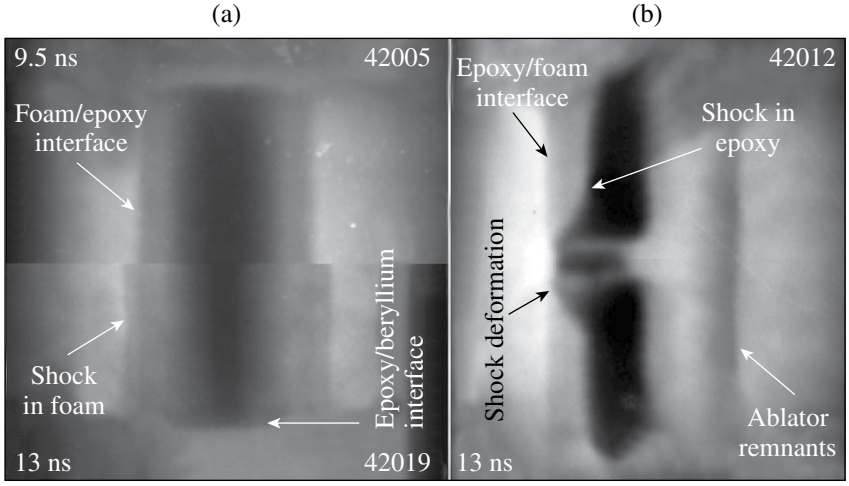

U613JR

Figure 108.96
(a) Radiographs of a heated-only, epoxy disk at 9.5 and 13.0 ns after the onset of heating. The deformation in the beryllium/epoxy interface and the shock formed by the epoxy expansion are both clearly visible. (b) Data from a heated and shocked 37.5-μm rectangular gap.

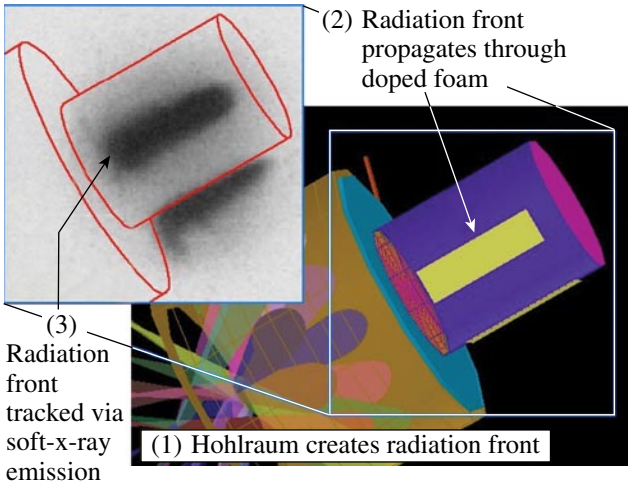

U614JRC

Figure 108.97
Sixteen beams heat a gold hohlraum that produces a radiation front that propagates through the foam. Diagnostic slits allow measurement of the front's progression.

of the temperature front (solid line). The simulation appears to be in good agreement with the data.

Beryllium Fill-Tube Defect Studies: Be shells are impermeable to gaseous and liquid DT. To fill an ICF capsule with a Be shell, a fill tube is used. The fill tube is attached to the shell through a counter-bored fill hole. Fill tubes and fill-tube holes for Be ICF capsules inject shell material into the fuel perturbing the implosion. Mixing between the shell material and the fuel cools the fuel and degrades the efficiency of the ICF capsule.

As part of the LANL/LLNL NIC effort, experiments designed to quantify the amount of Be mass ejected by the jet formed by the fill-tube hole were conducted. These experiments were performed in planar geometry due to complications of fabricating and diagnosing in spherical geometry. This experiment focused on large-aspect-ratio (depth/diameter), from 2 to 20, holes. The experimental configuration is shown in Fig. 108.99. A hohlraum is heated to 170- to 180-eV temperature. The temperature drive ablates and shocks the 100-μm-thick Be (3% Cu–doped) ablator. The shock ejects some material down the fill-tube hole and also propagates into the Be (3% Cu–doped) washer. The shock in the washer pushes material into the hole that jets into the foam.

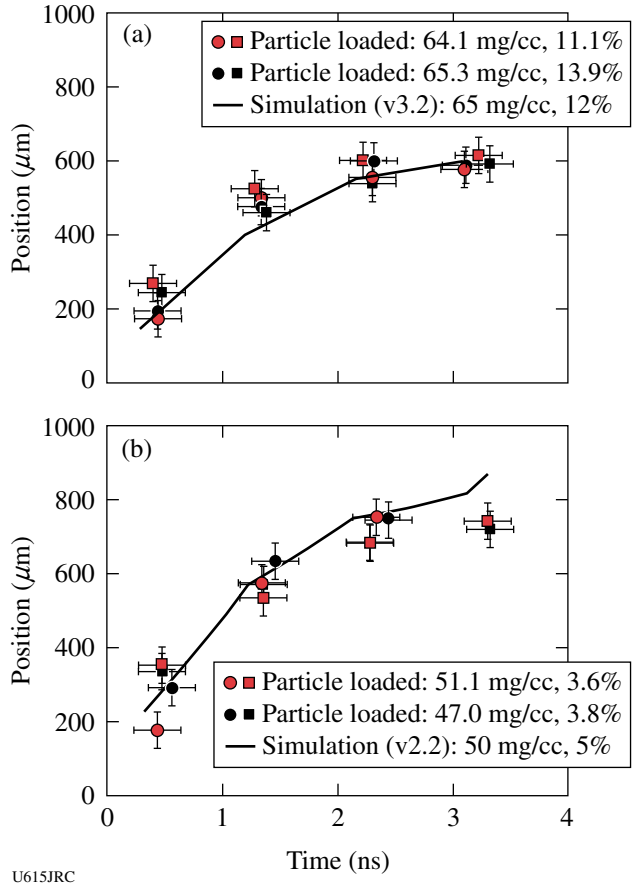

Figure 108.98
Simulations using NYM are in excellent agreement with the two cases examined: (top) 65-mg/cc foam with approximately 12% gold by weight and (bottom) 50-mg/cc foam with 5% gold by weight. [NYM simulations courtesy of M. Taylor (AWE).]

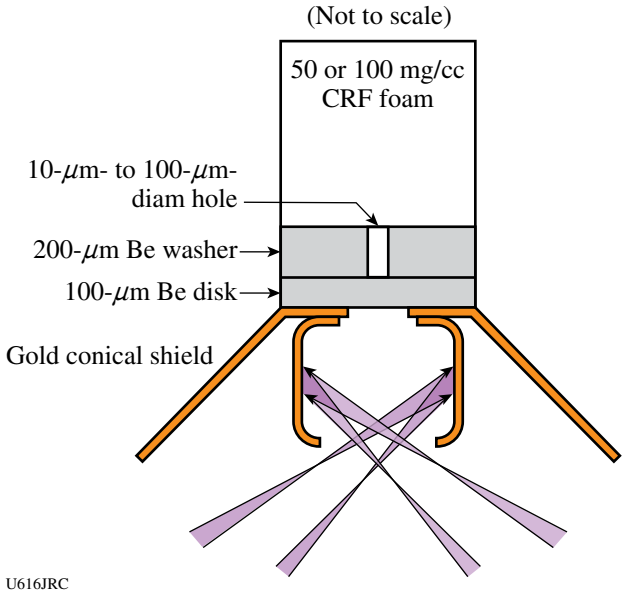

Figure 108.99
A heated gold hohlraum drives a shock into the beryllium disk, creating a jet as the Be is forced out the small hole at the bottom. The Be jet and disk are imaged from two orthogonal directions.

The mass of material jetted into the foam is measured with point-projection radiography at either 4.3 keV or 2.8 keV. Data have been obtained for jets formed by 100-, 50-, 40-, and 30-μm-diam holes. Figure 108.100 shows preliminary data of the jet formed by a 50-μm-diam fill-tube hole. The data were recorded with 4.3-keV x rays, 15 ns after the laser drive. The jet is roughly 170 μm across at the head and approximately 170 μm in length.

High-Z Shell Implosions: Two days of experiments studied the progression from non-LTE to LTE as the dopant gas concentration in a deuterium-filled capsule is increased. The presence of the high-Z dopants increases the radiation losses from the plasma, allowing the plasma to compress to a smaller volume. The physics of ignition and burn in high-Z capsules—specifically the effect of high-Z dopants on energy balance, equilibration, yield, and transport in implosions—is examined with measurements of yield, ρR, T_e, T_i, T_r, and implosion size.

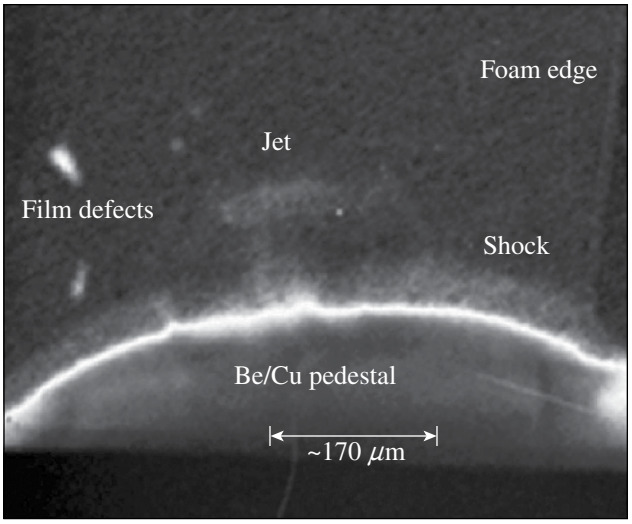

Figure 108.100
The jet caused by a 50-μm-diam hole taken 15 ns after onset of the laser drive. Visible are the jet and the shock wave that has passed through the Be. The radiograph was obtained with 4.3-keV x rays.

These experiments used a 5-μm-thick SiO_2 spherical shell of 430-μm radius, filled with 7 atm of deuterium and 3 atm of ^{3}He. The ^{3}He allows measurement of the proton spectrum from the D^{3}He reaction and thus determines the target's ion temperature and ρR. Kr dopants were used as spectroscopic tracers to measure the electron temperature in the plasma from the helium lines. Variation of electron density is achieved by adjusting the Xe gas concentration. The experiments produced a wealth of data that is being used to determine how equilibrium is reached and to validate code calculations (Fig. 108.101).

High-Z Dopant Impact in Stimulated Raman Scattering (SRS): Experiments at the Helen laser observed a clear decrease in stimulated Raman backscattered (SRS) light when a small percentage, ~1%–2%, of a high-Z dopant such as Ar or Xe was added to a CH-filled gas-bag target. This experimental observation prompted interest in the phenomenon, especially as a mitigation strategy for reducing SRS in NIF hohlraums. However, the exact physical mechanism of the high-Z dopant effects was unknown, especially the fact that only small amounts of high-Z dopant are required. Theoretical investigation of the effects of high-Z dopants on SRS at LANL found that the addition of high-Z dopants leads to beam spray of the laser via thermally enhanced forward stimulated Brillouin scattering (FSBS). This beam spray causes a reduction is SRS due to a reduction in the spatial coherence of the laser. Thermal effects due to inverse-Bremsstrahlung absorption of the laser have a Z^2 dependence, meaning that a small amount of high-Z material, compared to the background plasma Z, can have a large effect on the thermal response.

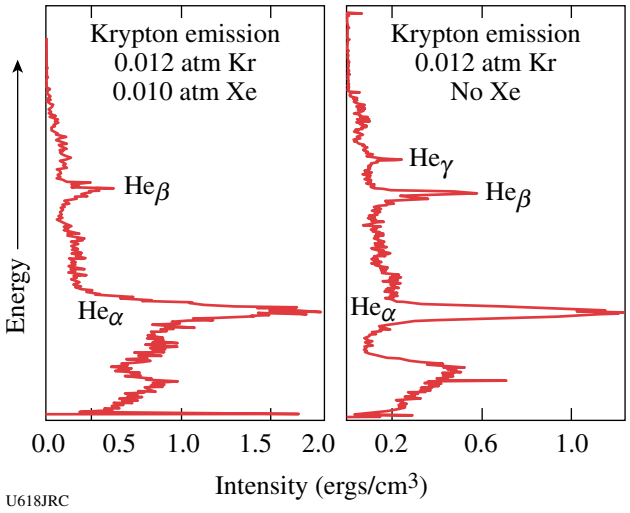

Figure 108.101
13- to 15-keV Krypton spectra of implosions doped (left) and undoped (right) with Xe. The enhanced cooling from Xe emission is observed by the reduction in He_γ and He_β emission of the Krypton spectra.

Through a strong collaboration by LANL, LLNL, and AWE, experiments were conducted at LLE using C_5H_{12} gas-filled hohlraum targets to validate theory. SRS was measured for various amounts of Xe dopant added to the hohlraum gas fill. As the percentage of Xe dopant exceeded ~5%, SRS from the uniform interior hohlraum plasma region decreased. Figure 108.102 shows that the SRS reflectivity at wavelengths of ~550 nm, corresponding to an electron density of $n/n_c \sim 0.11$, where n_c is the critical density for 351-nm light, is reduced with the addition of 8.7% Xe compared to that of 3.6% Xe early in the interaction-beam laser pulse. This is an indication that high-Z dopants may affect SRS. However, measurements of the beam spray for the transmitted beam did not change significantly between the two cases. Thus, it is inconclusive whether the effect is due to beam spray or another mechanism such as reabsorption of SRS light via inverse Bremsstrahlung. Interestingly, large amounts of SRS come from the plasma expanding from the hohlraum based on hydrodynamic simulations and the wavelength of SRS at ~520 nm corresponding to an electron density $n/n_c \sim 0.06$.

In FY07 experiments, the laser intensity will be lowered to values closer to the critical onset intensity for SRS. The theory predicts a stronger effect of high-Z dopants at that intensity. In addition, the SRS reflectivity from the plasma expanding from the hohlraum should be decreased based on past experiments at the NOVA laser.

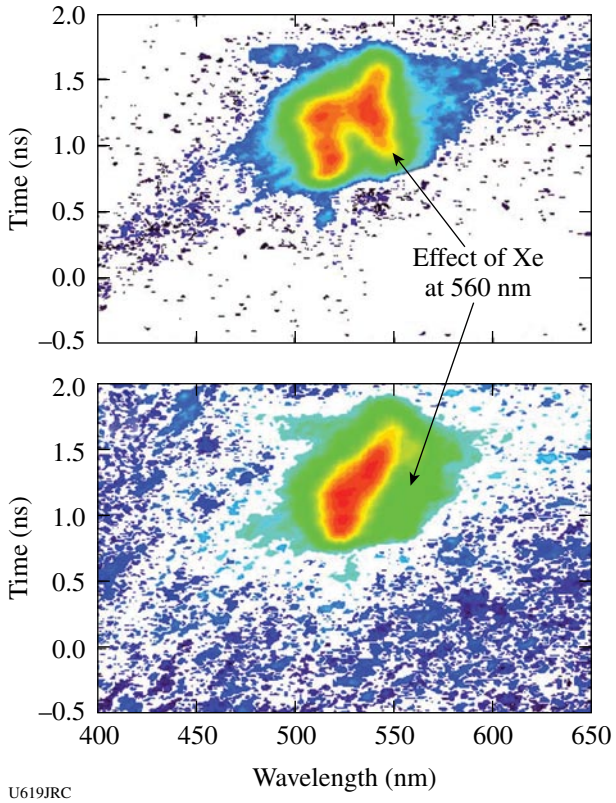

Figure 108.102
SRS spectra with (a) 3.6% and (b) 8.7% Xe dopant added to C_5H_{12} gas-filled hohlraums show a reduction in reflectivity at the interior electron density of $n/n_c \sim 0.11$ (~550 nm). However, most of the SRS reflectivity comes from the plasma expanding from the hohlraum at a lower electron density, $n/n_c \sim 0.06$ (~520 nm).

Gas Cherenkov Detector Development: The Gas Cherenkov Detector (GCD) is a collaborative effort between LANL, AWE, Photek, Inc., and NSTec to develop a fast "bang-time" diagnostic for NIF. The project benefited greatly from the multi-institutional diagnostic development efforts in FY06. Implementation of an ultrafast microchannel plate enhanced time response by a factor of 2.5 to better than 100 ps. This increased bandwidth enabled quality reaction histories of fusion burn using gammas (Fig. 108.103) to be obtained with speeds comparable to or exceeding that of the neutron temporal diagnostic (NTD). Moreover, bang-time measurements, i.e., the time of peak fusion reactivity, were achieved with a precision of 25 ps, when cross calibrated to NTD. This development should allow the gamma bang time/reaction history detector being planned for NIF to easily exceed the NIF system design requirement of 50 ps. The bang-time measurements, shown in Fig. 108.104, were obtained over a three-month period starting in May and ending with the 50/50 DT Cryo shots in July.

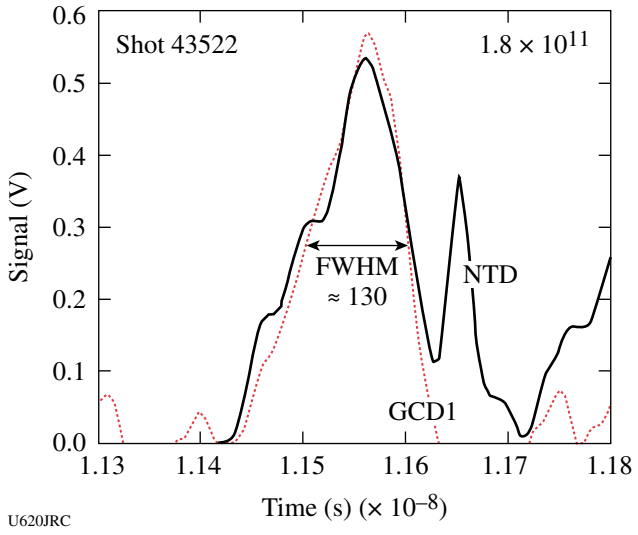

Figure 108.103
Gamma (GCD) and neutron reaction history (NTD) showing the consistency between burn history and peak neutron bang time.

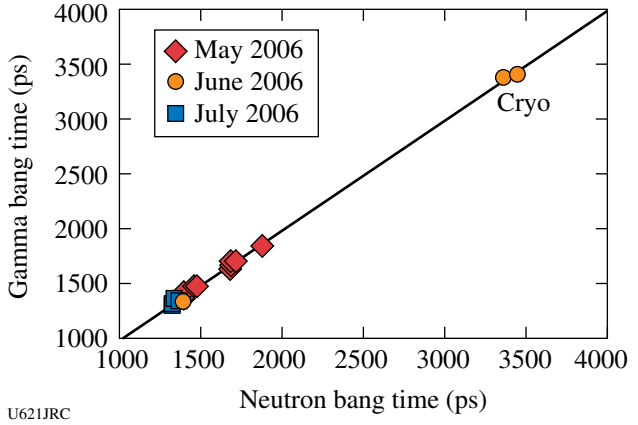

Figure 108.104
Peak-neutron-bang-time measurements of GCD and NTD are consistent over a wide time window.

FY06 Sandia National Laboratories OMEGA Experimental Programs

SNL carried out 30 shots on OMEGA in FY06 including the following experiments:

Beryllium Ablation Rate Measurements in Planar Geometry: For a successful NIF ignition experiment, the ablator mass remaining at the end of the capsule implosion must be in the range of 3%–5% of the original ablator mass. If too much of the ablator burns off, the DT fuel will be preheated and the required fuel ρR cannot be achieved with the absorbed energy of the baseline ignition capsule. If too little of the ablator mass

burns off, the peak implosion velocity will be reduced and the hot-spot energy density will not be adequate for ignition. Thus, it is imperative that the mass ablation rate be known to high precision for the entire range of hohlraum temperatures encountered in the NIF ignition pulse shape. The experimental technique for ablation rate measurements in planar geometry is illustrated in Fig. 108.105 (details in Ref. 9). Basically, ablator samples are placed over an opening on the end of a halfraum. Laser beams enter through the LEH and provide the input power required to maintain the radiation field. The Dante array of K- and L-edge filtered photocathodes views the hohlraum wall through the LEH, and a time- and spectrally resolved measurement of the hohlraum radiation field is obtained from this data. An x-ray framing camera views the interior surface of the ablator sample, and the relative x-ray re-emission of the ablator versus the Au wall is determined. The streaked x-ray imager (SXI) diagnostic views the exterior surface of the ablator sample. The SXI employs an imaging slit, a transmission grating, an offset slit, and a streak camera to provide a highly time-resolved streaked image of the x-ray burnthrough flux on the exterior-facing side of the sample (as shown in Fig. 108.105). The combined information from these three measurements over a series of experiments is used to determine the mass ablation rate (mg/cm^2/ns) as a function of hohlraum radiation temperature. In FY06, reduced-scale halfraums and increased SXI magnification were used to extend the ablation rate data for Be and Cu-doped Be into the 200- to 270-eV temperature range. As shown in Fig. 108.106, the measurements have been directly compared to the equivalent mass ablation rate in the baseline NIF ignition capsule calculations.[10–12]

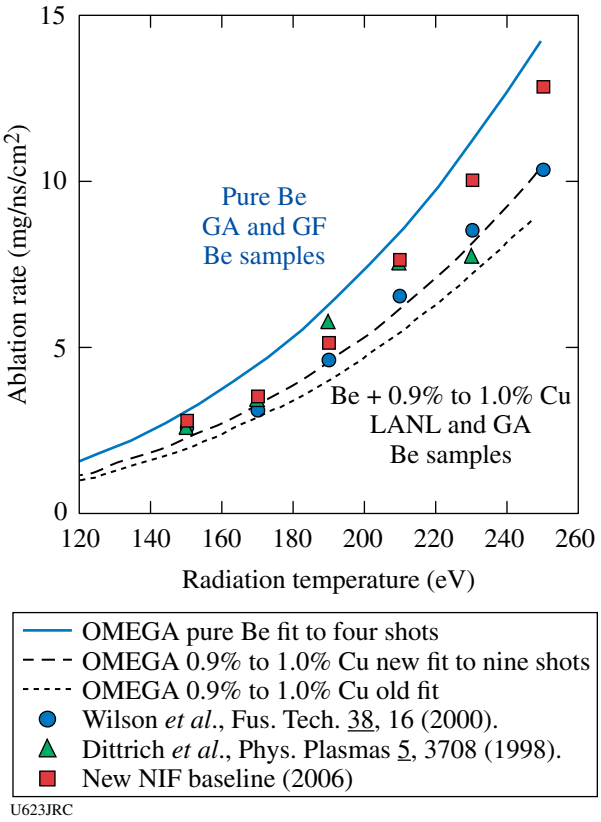

Figure 108.106
Ablation rate plotted as a function of radiation temperature from the OMEGA experiments (solid and dashed lines) and comparison to the baseline NIF capsule calculation. The range in the measured ablation rate seems to depend on view factor and spectrum as well as sample type and dopant concentration. Complete understanding of this data is work in progress.

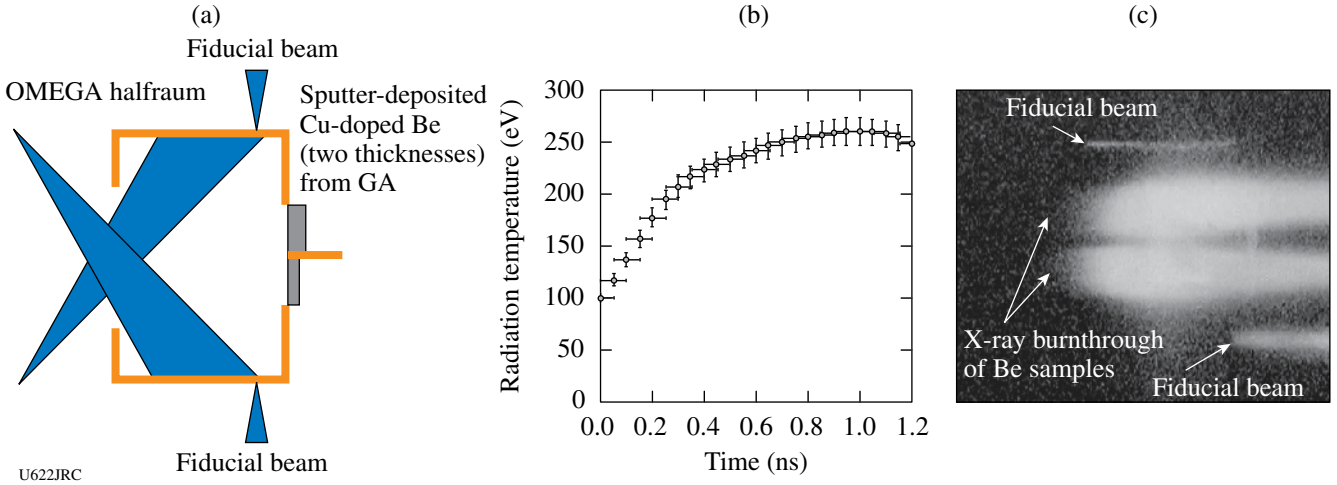

Figure 108.105
(a) Schematic of an ablation-rate measurement experiment. (b) DANTE-derived radiation temperature as a function of time. (c) Sample SXI streaked data showing burnthrough of Be samples.

Beryllium X-Ray Burnthrough and Ablation-Rate Measurements in Convergent Geometry: Since the ignition capsule's radius-time trajectory will vary with the shock-timing adjustments, it will be necessary to experimentally determine the burnthrough/no-burnthrough threshold of an imploding ablator shell and to iterate this burnthrough threshold measurement with the NIF shock-timing experiments. In FY06, SNL performed a series of experiments to develop a convergent ablation rate and burnthrough measurement technique. As illustrated in Fig. 108.107, the convergent burnthrough experiments are a logical extension of the planar ablation rate experiments. In the convergent experiments, a beryllium hemi-shell was mounted in a halfraum. The halfraum was larger than the sizes used in planar experiments, and specific beam-pointing adjustments were required to obtain acceptable capsule illumination symmetry (<±5% in flux). An important diagnostic concern was that pinhole SXI imaging (rather than slit imaging) was required for the convergent measurement, and a new technique was developed to verify the pointing and alignment accuracy to within ±50 μm. The SXI pinhole imaging setup is illustrated in Fig. 108.108, and the alignment verification technique is illustrated in Fig. 108.109. Key features of the burnthrough and no-burnthrough SXI streaks were verified in the FY06 experiments, and a preliminary unfold of convergent ablation rate was obtained from one of the experiments. Figure 108.110 shows an example x-ray streak image illustrating the spatial and time fiducials and an overlay of computationally simulated ablation-front and implosion features.

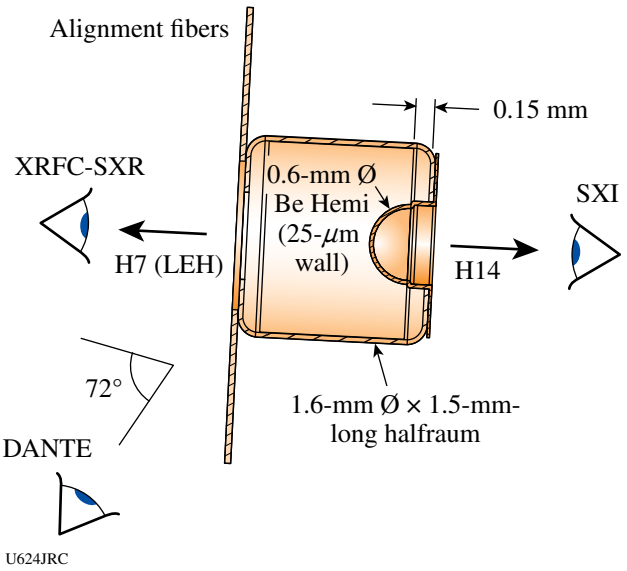

Figure 108.107
Illustration of a convergent burnthrough experiment.

VISAR Measurement of Hohlraum Radiation Temperature: In FY05, a new technique for time-resolved measurement of hohlraum radiation temperature was successfully tested in a series of OMEGA experiments.[13] In FY05, we performed a series of experiments to extend the measurement techniques of Ref. 13 to situations in which shaped laser pulses have been used to produce sudden increases in the hohlraum radiation field, resulting in multiple shock fronts that converge within the quartz sample. As can be seen in Fig. 108.111, the interferometer technique appears to work well for this situation. Based on FY06 results, it is conceivable that a new series of Dante-interferometer calibration shots can be used to produce empirical relationships for the situation of multiply shocked quartz.

Development of a NIF Shock-Timing Diagnostic: The x-ray flux absorbed by an indirect-drive ICF capsule consists of a combination of blackbody x rays emitted from the high-*Z* hohlraum walls and higher-energy (>1 keV) x rays that originate in and near the hot, low-density plasma in which the laser light is absorbed. The high-energy photons can penetrate beyond the capsule. In previous LLE/SNL/LLNL collaborative experiments,[14] we found that, as hohlraum temperatures were increased beyond 135 eV, the ASBO window was preheated and became opaque. In the first half of FY06, the approach was to position the window completely out of the

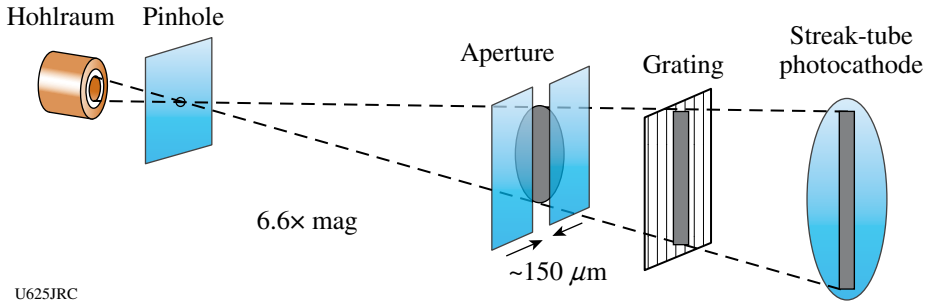

Figure 108.108
Schematic showing SXI pinhole imaging setup.

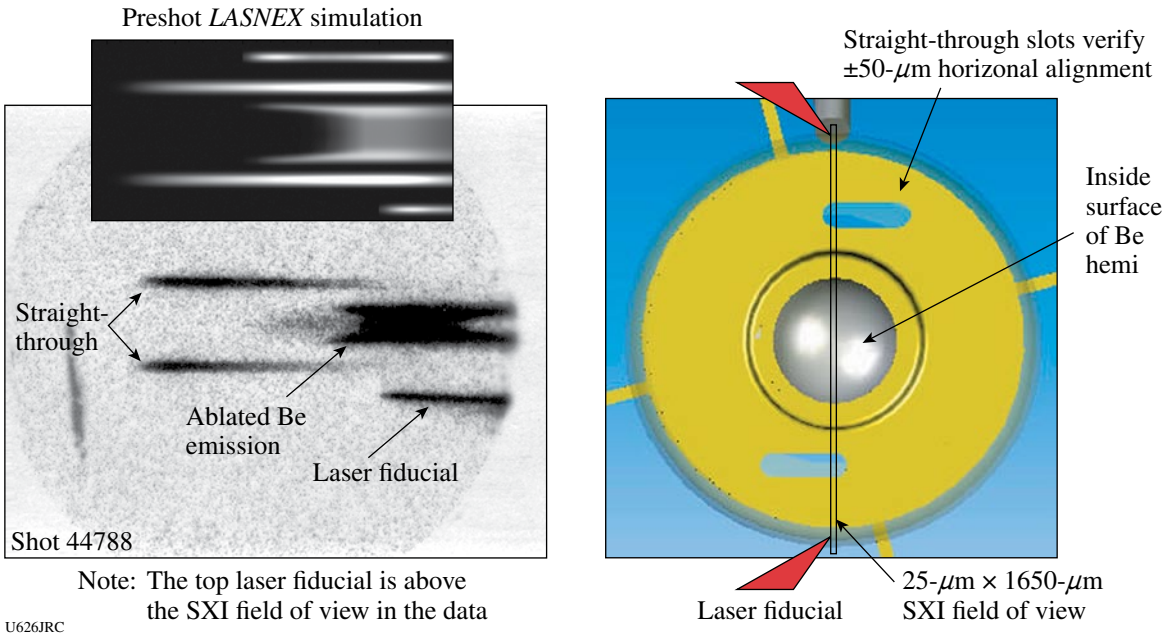

Figure 108.109
Illustration of the alignment verification technique.

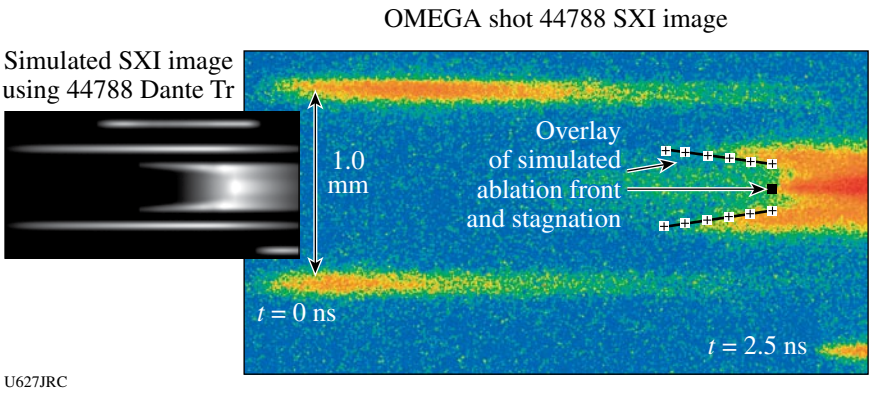

Figure 108.110
Sample SCI data (right) and simulation from a convergent breakthrough experiment (left).

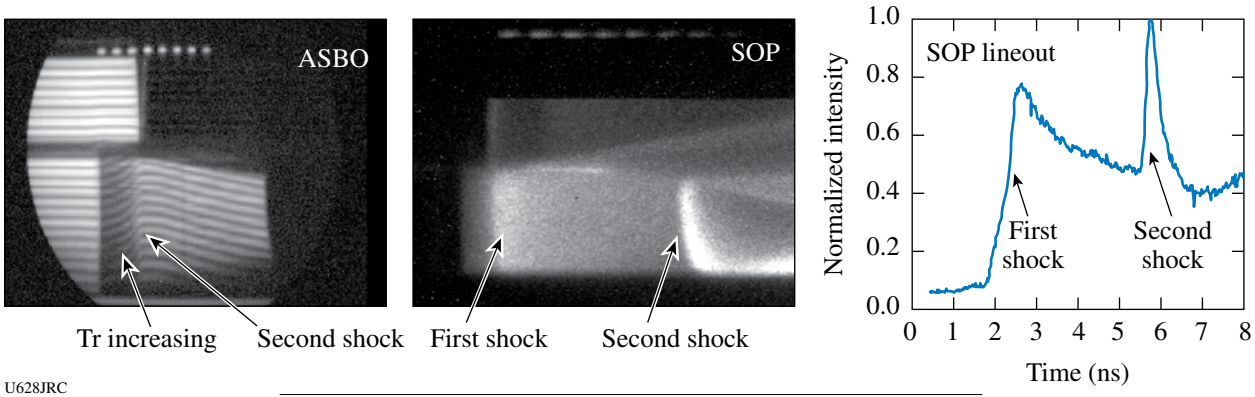

Figure 108.111
Illustration of the VISAR technique to measure hohlraum radiation temperature.

line of sight of the laser spots in a halfraum geometry. This approach improved the situation and resulted in successful ASBO measurements for halfraum temperatures exceeding 140 eV (see Fig. 108.112). In late FY06, a series of experiments was started in which a NIF-like shock-timing geometry was tested. The first so-called "line-of-sight" hohlraum targets (Fig. 108.113) were designed and assembled at SNL. The targets worked well, but the experimental results indicated that further refinements in the design will be required for a successful shock-timing technique.

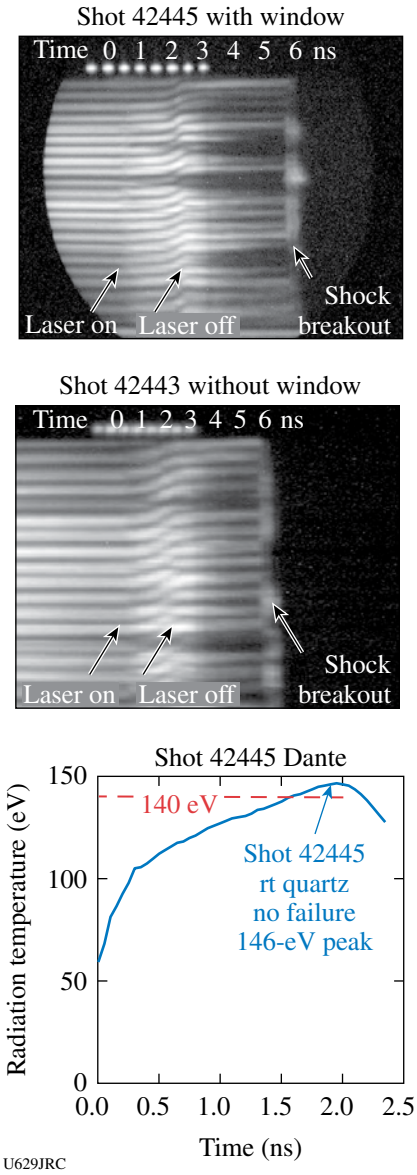

Figure 108.112
Illustration of successful ASBO measurement in radiation fills exceeding 140 eV.

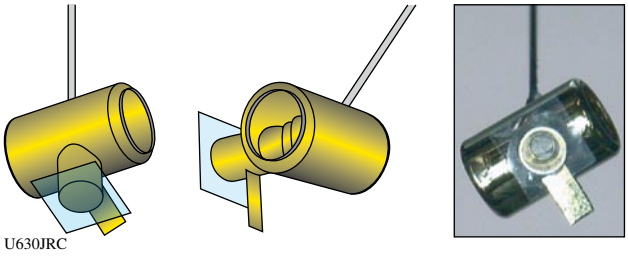

Figure 108.113
Schematic of hohlraum used to test a NIF-like shock-timing geometry.

FY06 CEA OMEGA Experimental Programs

In FY06, CEA carried out 49 target shots on OMEGA on several campaigns including studies of Rayleigh–Taylor instabilities in indirect-drive targets and the implementation of high-resolution x-ray imaging. Some of this work is outlined in this section.

Rayleigh–Taylor Instabilities in Indirect Drive: Mode-Coupling Experiments: Rayleigh–Taylor instabilities in indirect drive have been investigated by CEA on OMEGA since 2002 by using a rugby wall-shaped hohlraum.[15] Rugby hohlraums are, in fact, alternative designs for pre-ignition experiments with reduced energy on LMJ,[16] and the control of symmetry in a rugby hohlraum was also one of the goals of CEA FY06 symmetry experiments. A sketch of a rugby hohlraum is shown in Fig. 108.114 together with a diagram of the experimental configuration used for the RTI experiments. The cavity is heated with 40 beams (pulse shape PS26) in a three-cone (21°, 42°, and 59°) irradiation scheme. The 21° beams propagate across the hohlraum and are absorbed in the slanted part of the wall on the opposite side of the laser entrance hole. Dual-axis radiographies (side-on and face-on) are performed on each shot to measure the foil acceleration and the perturbation growth.

Previous experimental campaigns were devoted to the measurement of single-mode RT growth rate (wavelengths λ = 50 and 70 μm) and the study of the feedout mechanism[17] in the case where the modulations were placed on the cold face [rear side, Fig. 108.114(a)] of the radiatively driven plastic foils.

The FY06 campaign focused on mode coupling with germanium-doped foils (CHGe, 2.8% in atomic weight) modulated front side with a two-mode pattern (λ = 35 and 70 μm). Depending on the relative phase between the two modes (in phase or in opposite phase), one or the other wavelength is predicted to become predominant during the growth. As illustrated in Fig. 108.115, if we compare two face-on pictures taken at the same time after t_0 (t = 2.7 ns), one sees clearly on the lineouts that

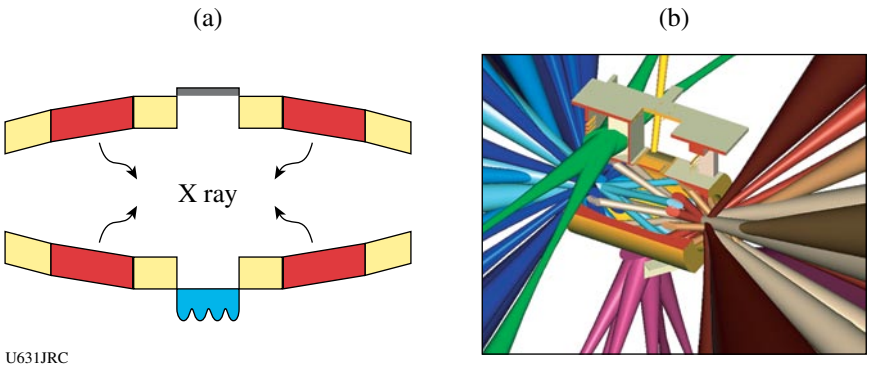

Figure 108.114
(a) Sketch of a rugby hohlraum. (b) Diagram of the configuration for RTI experiments. The 21° beams propagate across the cavity and are absorbed in the slanted part of the wall on the opposite side of the laser entrance hole.

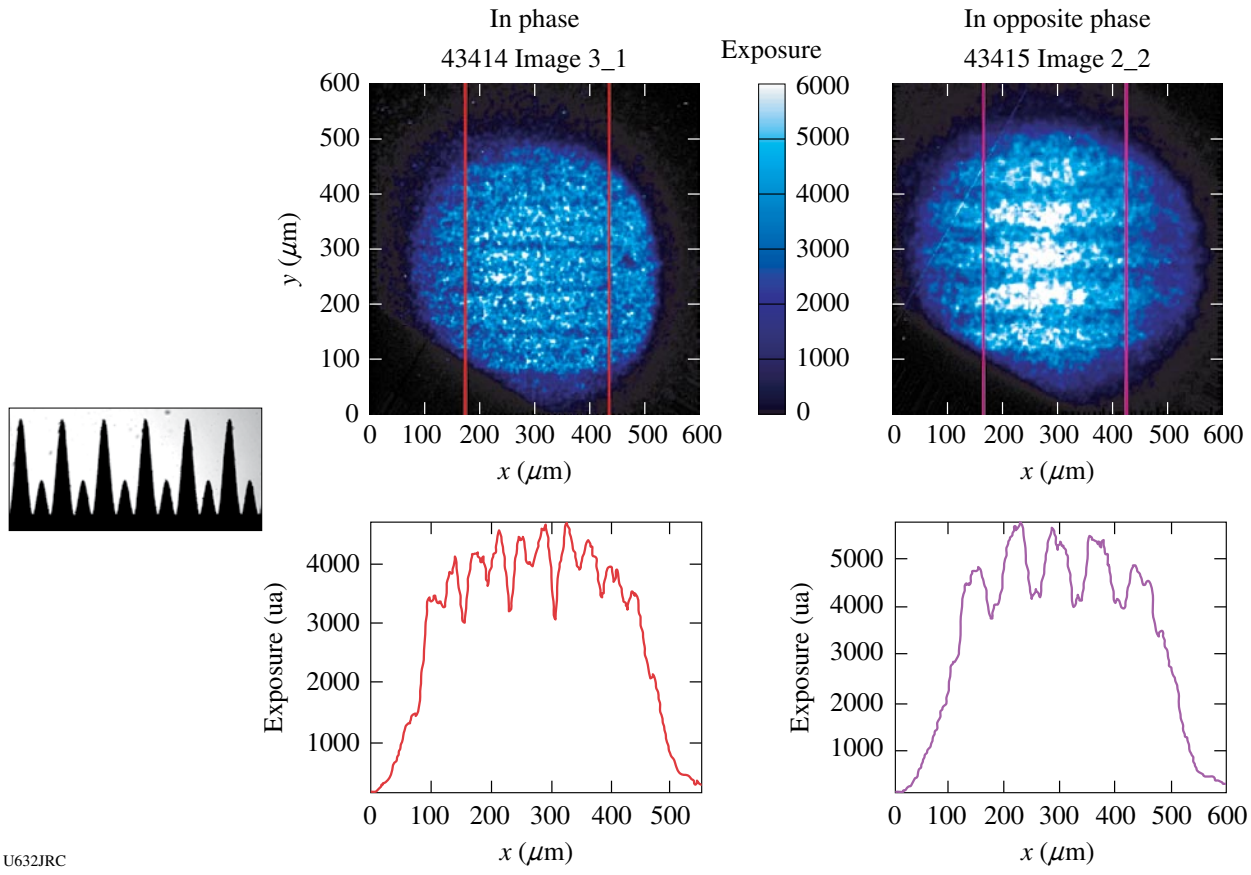

Figure 108.115
Lineouts across two face-on pictures taken at the same time ($t = 2.7$ ns) for the two-mode patterns ($\lambda = 35$ and 70 μm) under study. On the left, in phase pattern with the preponderant $\lambda = 35$-μm mode. On the right, the opposite phase pattern where $\lambda = 70$ μm predominates.

the λ = 35-μm mode overwhelms the λ = 70-μm mode for the in-phase case, and inversely for the opposite-phase pattern. As a consequence, the growth of the λ = 35-μm mode in the opposite-phase pattern is predicted to be delayed in time (due to a phase inversion) in comparison with a pure λ = 35-μm monomode. This trend is recovered in Fig. 108.116 on the plot showing the evolution of the optical depth versus time for both cases.

High-Resolution X-Ray Imaging (HRXI): For several years, Commissariat à l'Énergie Atomique in France (CEA/DIF Center[18]) has been developing HRXI, a high-resolution, time-resolved, x-ray imaging diagnostic. In FY06, HRXI was implemented and tested for the first time on OMEGA. HRXI combines two state-of-the-art technologies: a high-resolution x-ray microscope and a high-speed x-ray streak camera. The resulting instrument achieves a spatial and temporal resolution of ~5 μm and ~30 ps, respectively. The experimental configuration is shown in Fig. 108.117. The Wolter x-ray microscope for HRXI, used previously on Phebus experiments,[19] consists of two similar off-axis toroidal mirrors. The microscope had a focal length of 218 mm and a magnification ratio of 16. The mirrors were coated with a 30-nm Ni coating (energy cutoff ~6 keV). The microscope features an integrated visible-light alignment system enabling the simultaneous projection of two crosses in the object plane and the image plane.

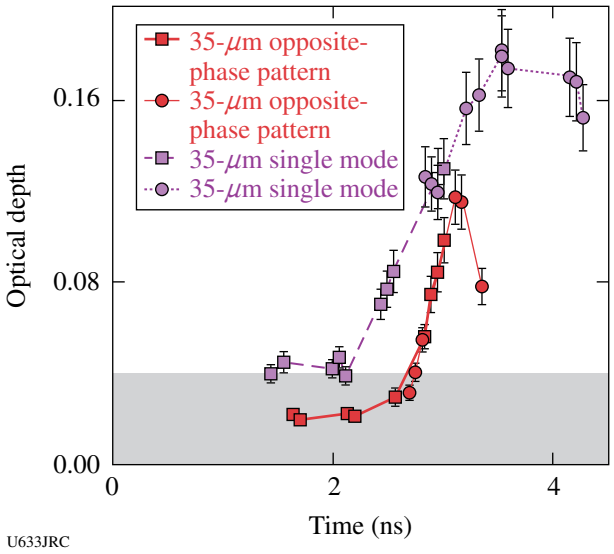

Figure 108.116
Growth (in optical depth) of the λ = 35-μm mode for the opposite phase pattern (solid symbols) and for a pure monomode perturbation (open symbols).

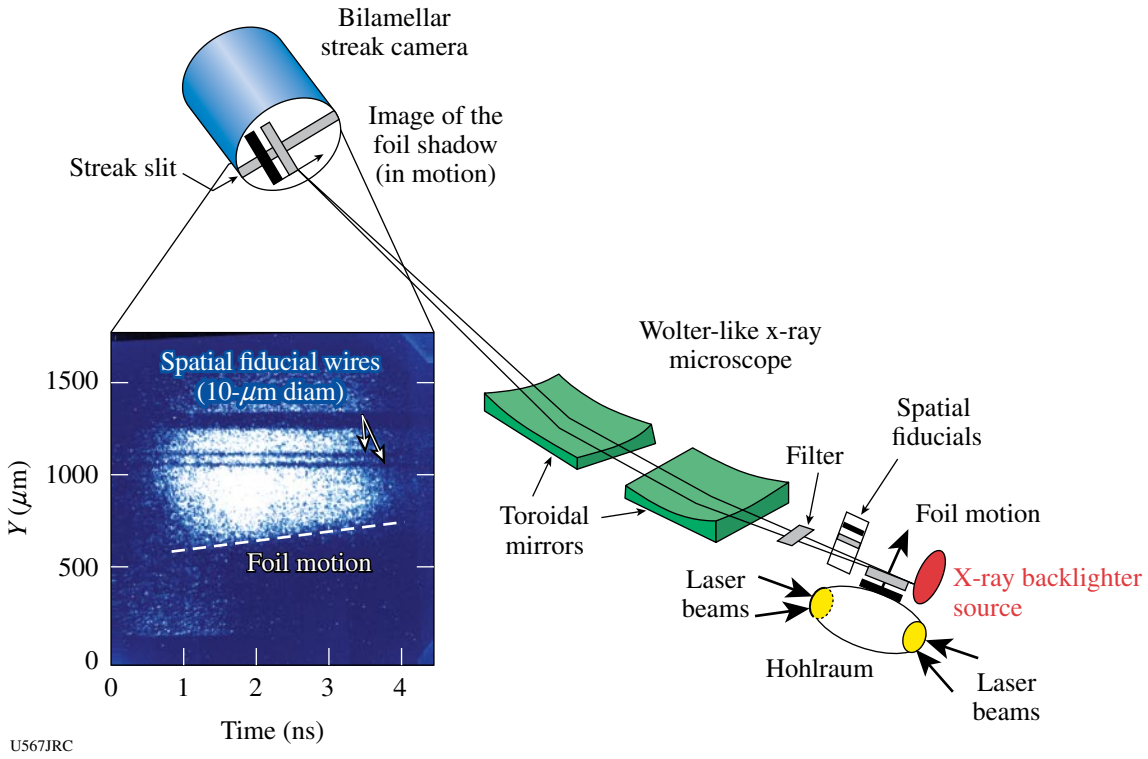

Figure 108.117
HRXI setup with a streaked image recorded during OMEGA shot 43418.

The streak camera includes a bilamellar-type streak tube,[20] which achieves both high temporal (30 ps) and spatial resolution (15 lp/mm). To match to the emitted x-ray backlighter spectrum used for these experiments (Ti foil emission near 4.8 keV), a transmission-mode photocathode was used with a thin CsI coating (10 nm) that was deposited on a self-sustaining CH foil of 800-nm thickness. The streak tube's P20 phosphor screen was read out with a cooled 1340×1300-pixel CCD with a 20-μm pixel size.

HRXI was sucessfully tested for the first time on OMEGA during a joint CEA/DOE-LLE campaign on 27 April 2006. For these tests, HRXI recorded the acceleration of a thin, Ge-doped CH (45-μm) foil driven by radiation from a rugby-wall–shaped hohlraum heated by 40 OMEGA beams with a 2-ns-time-duration, PS26 pulse shape. The foil was accelerated to a velocity of 60 μm/ns. The inset in Fig. 108.117 shows a streak record of the motion of this thin foil in time using a 3-ns x-ray backlighter source. Three test objects were placed close to the foil to assess the spatial resolution of the diagnostic. Two 10-μm-diam wires are clearly visible in the middle and along the streak image, leading to an actual estimated spatial resolution on the streaked image of less than 5 μm.

REFERENCES

1. R. F. Smith *et al*., "Stiff Response in Aluminum Under Ultrafast Shockless Compression up to 110 Gpa," submitted to Physical Review Letters.
2. S. D. Rothman *et al*., J. Phys. D **38**, 733 (2005).
3. R. F. Smith *et al*., "Graded-Density Reservoirs for Accessing High Pressure Low Temperature Material States," to be published in Astrophysics and Space Science.
4. R. Jeanloz, Geophys. Res. Lett. **8**, 1219 (1981).
5. M. H. Rice, R. G. McQueen, and J. M. Walsh, Solid State Phys. **6**, 1 (1958).
6. C. K. Li, F. H. Séguin, J. A. Frenje, J. R. Rygg, R. D. Petrasso, R. P. J. Town, P. A. Amendt, S. P. Hatchett, O. L. Landen, A. J. Mackinnon, P. K. Patel, V. A. Smalyuk, T. C. Sangster, and J. P. Knauer, Phys. Rev. Lett. **97**, 135003 (2006).
7. C. K. Li, F. H. Séguin, J. A. Frenje, J. R. Rygg, R. D. Petrasso, R. P. J. Town, P. A. Amendt, S. P. Hatchett, O. L. Landen, A. J. Mackinnon, P. K. Patel, V. Smalyuk, J. P. Knauer, T. C. Sangster, and C. Stoeckl, Rev. Sci. Instrum. **77**, 10E725 (2006).
8. D. H. Froula *et al*., Phys. Plasmas **13**, 052704 (2006).
9. R. E. Olson, R. J. Leeper, A. Nobile, J. A. Oertel, G. A. Chandler, K. Cochrane, S. C. Dropinski, S. Evans, S. W. Haan, J. L. Kaae, J. P. Knauer, K. Lash, L. P. Mix, A. Nikroo, G. A. Rochau, G. Rivera, C. Russell, D. Schroen, R. J. Sebring, D. L. Tanner, R. E. Turner, and R. J. Wallace, Phys. Plasmas **11**, 2778 (2003).
10. D. C. Wilson *et al*., Fusion Technol. **38**, 16 (2000).
11. T. R. Dittrich *et al*., Phys. Plasmas **5**, 3708 (1998).
12. S. W. Haan *et al*., Fusion Sci. Technol. **49**, 553 (2006).
13. R. E. Olson *et al*., Rev. Sci. Instrum. **77**, 10E523 (2006).
14. R. E. Olson, R. J. Leeper, G. A. Rochau, D. K. Bradley, P. M. Celliers, and T. R. Boehly, J. Phys. IV France **133**, 179 (2006).
15. A. Casner *et al*., J. Phys. IV France **133**, 163 (2006).
16. J. Giorla *et al*., Plasma Phys. Control. Fusion **48**, B75 (2006).
17. D. P. Smitherman *et al*., Phys. Plasmas **6**, 932 (1999).
18. J. L. Bourgade *et al*., CEA/DIF Center, Service SCEP, BP 12, Bruyères le Châtel, 91680, France.
19. Ph. Troussel *et al*., Rev. Sci. Instrum. **76**, 063707 (2005).
20. A. Mens *et al*., in *19th International Congress on High-Speed Photography and Photonics*, edited by B. Garfield and J. Rendell (SPIE, Bellingham, WA, 1990), Vol. 1358, pp. 315–328.